positively charged groove at the concave side of RD that colocalizes with a region of high sequence conservation. To analyze this putative RNA 5′-triphosphate recognition site, we tested a variety of RD mutants in this region for interaction with pppRVL, using our fluorescence anisotropy assay (Figures 6C and 6D and Table S3).

Two control mutations (K807A and D836A), located on the convex side of RD, did not significantly alter the binding affinity for pppRVL, although these residues are highly sequence conserved. In contrast, three mutations in conserved residues inside the positively charged groove significantly reduced the binding affinity (H830A, I875A, and K888A). The mutation K858A, however, located at the center of the positive patch, dramatically reduced binding of pppRVL. This strong effect indicates that the groove is involved in the binding of the RNA 5′-triphosphate. We tested the K858A, K888A, and H830A mutants in vivo and found a significant reduction, but not complete abrogation of IFN-β promoter activity induced by transfection with pppVSVL or infection with VSV-M51R (Figure 6E, left). Mutations to negatively charged glutamates in the same positions (K858E, K888E, and H830E) entirely abrogated the response to pppVSVL and VSV-M51R (Figure 6E, right). The similar relative reductions in activity of the mutants in in vitro and in vivo experiments argue that the RNA binding defects observed in vitro are also the cause of reduced activity in vivo. Together, these observations suggest that interaction of VSV-RNA with the positively charged patch of the groove is required for full activation of RIG-I in vivo.

We do not see significant binding of fluorescently labeled UTP to RD (data not shown), which also contains a triphosphate. Thus, RD recognizes more than the triphosphate and sugar/base moiety of the 5′-terminal base of pppRNA. However, if RNA extends from K858 along the longest dimension of RD, the footprint will cover at most three bases, indicating that recognition of viral RNA by RD is limited to the very 5′-terminal region. This argues that adjacent 3′ regions could then bind to the RNA-binding sites of the DECH box domain.

Proposed Model for RD-Dependent RIG-I Activation

In summary, our data suggest a model for RIG-I activation that includes the following chain of events (Figure 6F). In the absence of 5′-triphosphate containing RNA ligands, RIG-I is monomeric and inactive. The CARDs probably partially mask an RNA-binding site on the DECH box domain. The preference of the DECH domain for dsRNA indicates that this RNA-binding site could also recognize secondary structures of virus RNA. pppRNA binding to RD induces a conformational change in the enzyme that results in dimerization and stimulation of the DECH box domain. The dimer form could, for instance, enable the binding of dsRNA or other types of RNA to the DECH domain by displacing the CARDs, and, in conjunction with or coupled to RNA-stimulated ATPase activity, this structural change might generate a signaling conformation of RIG-I. In analogy to adenosine triphosphate binding-dependent structural switches in many ATPases (Hopfner and Tainer, 2003), the binding energy of RNA 5′-triphosphates, which is likely in the same range as the binding energy of ATP to ATPases, is well suited to trigger such a macromolecular conformational change.

RIG-I RD mutants that have strongly reduced signaling activity are still able to interact with IPS-1 (Figure S8). We do not know at the moment how a RIG-I:IPS-1 interaction might lead to initiation of downstream signaling. Our dimerization results make it likely that the IPS-1:RIG-I signaling conformation includes a RIG-I dimer and for that reason possibly also an IPS-1 dimer. Because RD helps to stabilize an inactive conformation of CARDs (Saito et al., 2007), RD mutations might allow or even stimulate CARD exposure and thus IPS-1 interaction, but prevent pppRVL-induced RIG-I dimer formation and for that reason signal induction.

In conclusion, our data reveal the binding site for 5′-triphosphates on RIG-I, located on the C-terminal regulatory RD domain. At the center of this binding site is a RIG-I invariant lysine residue that is critically required for triphosphate binding. This lysine is partially buried, similar to the lysine in the P loop of NTPase, and this location is well suited for phosphate interaction. Interestingly, LGP2 contains a proline at the position of RIG-I K858, while MDA5 either contains a threonine or an isoleucine (Figure 4C). Consistent with this observation, we did not see strong binding of pppRVL to RDs of MDA5 and LGP2 (data not shown). Thus, RDs of MDA5 or LGP2 might either bind to different types of ligands or fulfill different functional roles. In any case, the RD of the three related DECH box ATPases could be an important specificity element. Thus, our results not only provide a structural framework to further analyze the specific recognition of viral RNA synthesis products by RIG-I, but could also to help to reveal the recognition of any ligands by the RDs of MDA5 or LGP2.

EXPERIMENTAL PROCEDURES

Protein Expression and Purification

RIG-I and MDA5 were expressed in insect cells as described previously (Berger et al., 2004). Briefly, cDNA was cloned into pFBDM vectors (MultiBac system, kindly provided by I. Berger) and transformed into DH10MultiBac cells. The bacmids were extracted for transfection into High-five insect cells (Invitrogen). Seventy-two hours after infection, the cells were harvested and lysed by "freeze and thaw." All other RIG-I and MDA5 constructs were expressed in *E. coli* BL21 Rosetta cells (Novagen), using pET expression vectors (Novagen). Cultures were grown at 37°C to an OD_{600} of 0.8. Expression was induced by addition of 0.5 mM IPTG, and cells were subsequently incubated at 18°C overnight, with shaking. After harvesting, resuspended cells were disrupted by sonication. All recombinant proteins were purified to homogeneity using metal affinity (QIAGEN) or Strep-Tactin fast flow (IBA), ion exchange, and gel filtration chromatography with standard protocols (GE Healthcare).

ATPase Assays

ATPase assay reaction mixtures (50 μl) contained 20 mM Tris-HCl (pH 7.5), 8 mM DTT, 5 mM $MgCl_2$, 10 mM KCl, 4% (w/v) glycerol, 80 μg/ml BSA, and the specified RNA (10 ng/μl) plus a trace amount of [γ-^{32}P]ATP (2 nM) mixed with different amounts of nonradioactive ATP and 20 nM enzyme. The

luciferase assay after 18 hr (fold induction compared to mock-treated empty vector control). Mean values and standard deviations (error bars) of three independent experiments are shown.

(F) Proposed model for RNA 5′-triphosphate (gray with red phosphates) activation of RIG-I by ligand-induced dimer formation of RD (yellow with magenta zinc ion). RNA stoichiometry and domain-domain interactions are tentative.

reactions were initiated by the addition of enzyme and incubated at 37°C. Samples (1 μl) were removed at 3 min intervals and evaluated by thin-layer chromatography. k_{cat} and V_{max} values were calculated by nonlinear curve fitting of multiple (two to five) independent determinations (see Table S2).

Molecular Weight Determination by Size-Exclusion Chromatography and Light Scattering

Assays were done on a GE Äcta system equipped with a Superose 6 10/300 (GE Healthcare) gel filtration column and connected to a Viscotek VE 3580 RI detector and Viscotek 270 DUAL detector. The gel filtration buffer was 30 mM Tris-HCl (pH 7.5), 150 mM NaCl, 2 mM DTT, and 10 μM $ZnCl_2$. UV absorption, refractive index, and low angle light scattering signals were collected. The system was calibrated with BSA (MW 67,000 Da) standard solution with a concentration of 2 mg/ml.

Fluorescence and Anisotropy Measurement

Fluorescence anisotropy experiments were performed with a FluoroMax-P fluorimeter (HORIBA Jobin Yvon), equipped with a Glan-Thompson prism polarizer. Typically, 1.2 ml of buffer (30 mM Tris-HCl [pH 7.5], 150 mM NaCl, 2 mM DTT, and 10 μM $ZnCl_2$) and 50 nM RNA (in vitro-transcribed pppRVL with incorporated Alexa Fluor 488-5-UTP) were pre-equilibrated in a quartz cuvette at 12°C. Protein samples were added in a stepwise manner and briefly mixed by magnetic stirring. After 3 min re-equilibration, the anisotropy data were collected using an excitation wavelength of 492 nm and monitoring the emission 516 nm. The band pass was 5 nm for excitation and 5 nm for emission. A maximum number of ten trials were performed until less than 2% deviation of the signal was reached.

In Vivo RD Titration Experiments

Reporter gene assays for activation of IFN-β promoter were performed in HEK293T cells seeded in 24-well plates. At a confluence of 75%, cells were transfected with 100 ng IFN-β firefly reporter plasmid (p125luc) and 1 ng of a plasmid encoding CMV-controlled renilla luciferase (pRL-CMV, Promega) as a control, using Lipofectamine 2000 (Invitrogen). In addition, cells were transfected with 100 ng of pEF-BOS-RIG-I full-length plasmid and the indicated increasing amounts of pCAGGS-RIG-I RD expression construct. Twenty-four hours after DNA transfection, cells were transfected with 200 ng in vitro-transcribed pppRVL to stimulate IFN production. Cells were lysed after 24 hr incubation and analyzed for dual reporter gene activity according to the supplier's instructions (Promega) in a Luminometer (Berthold).

In Vivo Analysis of RIG-I Mutants

HEK293 cells (DSMZ, Braunschweig, Germany) were maintained in DMEM with supplements (0.6 g/l L-Glu, 10% FBS, and 1% Pen/Strep from GIBCO-Invitrogen, Karlsruhe, Germany). BHK21 cells (ATCC) were grown in Glasgow medium supplemented with 0.6 g/l L-Glu, 10% FBS, 1% Pen/Strep, and 1% tryptose broth (GIBCO-Invitrogen). Cell cultures were incubated at 37°C with 5% CO_2. VSV-M51R mutant was kindly provided by O. Ebert (TU Munich). Virus stock and plaque assay on BHK21 cells have been described. Mutants of Flag-RIG-I (kindly provided by T. Fujita) were generated using the QuikChange Site-Directed Mutagenesis Kit (Stratagene, Amsterdam, Netherlands) and sequenced. HEK293 cells (2×10^5 cells/24-well) were transiently transfected with 10 ng of pRL-TK reporter (renilla luciferase under control of TK promoter, Promega, Mannheim, Germany), 100 ng of pIFN-β-Luc (firefly luciferase under control of mIFN-β promoter, kindly provided by T. Taniguchi), and 10, 100, or 400 ng of RIG-I constructs or empty control vector using Lipofectamine 2000 (Invitrogen, Karlsruhe, Germany). Eighteen hours after transfection, cells were either infected with 10 moi VSV-M51R or transfected with 1 μg/ml in vitro-transcribed pppVSVL or RNA isolated from mock-infected and VSV-infected cells using Lipofectamine 2000. Cell extracts were prepared and assayed in the Dual Luciferase Reporter System (Promega) after 18 hr.

RNA Pull-Down Experiments

5′-triphosphate RNA encompassing the VSV leader RNA sequence (pppVSVL) was generated by in vitro transcription from a template DNA generated by PCR using plasmid rVSV-EGFP (kindly provided by O. Ebert) as template and 5′ T7 primer (MAXIscript T7 Kit, Ambion, Huntingdon, UK). The DNA template was removed by DNase I treatment, and RNA was purified using Nuc Away Columns (Ambion). For removal of 5′-triphosphates, 20 μg of RNA was treated with 30 U CIAP (NEB, Frankfurt/Main, Germany) for 2 hr at 37°C in the presence of RNase inhibitor (Fermentas, St. Leon, Germany) and extracted with phenol-chloroform. Biotinylated pppVSVL was transcribed from the template DNA described above by using the AmpliScribe Flash T7 Kit (Epicenter, Madison, USA) and biotin-16-uridine-5′-triphosphate (Roche, Mannheim, Germany). RNA binding assays were performed as described (Saito et al., 2007): cytoplasmic extracts were prepared from 3×10^6 HEK293 cells transfected with Flag-RIG-I plasmids. The extracts were incubated with biotinylated pppVSVL and subjected to pull-down with streptavidin agarose beads (Sigma-Aldrich, Munich, Germany), followed by SDS-PAGE analysis and immunoblotting with anti-Flag M2 antibody (Sigma-Aldrich, Munich, Germany).

Crystallization and Structure Determination

RD was crystallized by mixing 2 μl protein (20 mg ml^{-1} in 30 mM Tris-HCl [pH 7.5], 150 mM NaCl, 2 mM DTT, and 10 μM $ZnCl_2$) with 2 μl buffer containing 0.1 M CHES (pH 10.0) and 18% w/v PEG 8000 in a sitting drop vapor diffusion system at 20°C. The derivative used for phase determination was prepared by soaking the crystals for 10 min in 2 mM mercury acetate, 0.1 M CHES (pH 10.0), and 18% w/v PEG 8000. Cryocooling was achieved by soaking the crystals for 5–10 s in reservoir solution containing 15% D(-)-2,3-butanediol and flash-freezing in liquid nitrogen. Highly redundant multiwavelength anomalous dispersion (MAD) data to 2.7 Å on mercury-containing and to 3 Å on native crystals were collected at beamlines PX SLS (Villigen, Switzerland) and ID23-2, ESRF (Grenoble, France). The data sets were processed with XDS (Kabsch, 1993). The space group was identified as P21, and 10 molecules were found per asymmetric unit. One mercury atom was located per molecule and initial phases were calculated and refined with the program AUTOSHARP (Global Phasing, Cambridge), leading to an interpretable electron density map. The manual model building was carried out by using the program Coot (Emsley and Cowtan, 2004). Prior to model building and refinement, we randomly omitted 10% of the reflections for monitoring the free R value. Refinement was performed with CNS V.1.1 (Brunger et al., 1998) and included overall anisotropic B factor and bulk solvent corrections, individual B factor refinement, simulated annealing, and positional refinement. Initial NCS restraints were gradually removed in the final cycles of the refinement, to allow some structural variations. Data collection and model statistics are summarized in Table 1. Figures were prepared with PyMOL (DeLano Scientific).

Supplemental Data

Supplemental Data include eight figures and three tables and can be found with this article online at http://www.molecule.org/cgi/content/full/29/2/169/DC1/.

ACKNOWLEDGMENTS

We thank Wolfgang Reindl for experimental help and Imre Berger for help with the MultiBac expression system. We thank the staffs of PXI (Swiss Light Source, Villingen) and ID14 (European Synchrotron Radiation Facility, Grenoble) for beam time allowance and help with data collection. This work was supported by the German Research Council DFG Sonderforschungsbereich 455 to K.-P.H., A. Krug, and K.-K.C. and by the Center for Integrated Protein Science and Munich Center for Advanced Photonics to K.-P.H. A. Kirchhofer acknowledges support by the DFG Graduate School 1202. This work is part of the theses of K.E. and A. Kirchhofer.

Received: April 6, 2007
Revised: July 12, 2007
Accepted: October 24, 2007
Published: January 31, 2008

REFERENCES

Akira, S., Uematsu, S., and Takeuchi, O. (2006). Pathogen recognition and innate immunity. Cell *124*, 783–801.

Berger, I., Fitzgerald, D.J., and Richmond, T.J. (2004). Baculovirus expression system for heterologous multiprotein complexes. Nat. Biotechnol. *22*, 1583–1587.

Brunger, A.T., Adams, P.D., Clore, G.M., DeLano, W.L., Gros, P., Grosse-Kunstleve, R.W., Jiang, J.S., Kuszewski, J., Nilges, M., Pannu, N.S., et al. (1998). Crystallography & NMR system: a new software suite for macromolecular structure determination. Acta Crystallogr. D Biol. Crystallogr. *54*, 905–921.

Emsley, P., and Cowtan, K. (2004). Coot: model-building tools for molecular graphics. Acta Crystallogr. D Biol. Crystallogr. *60*, 2126–2132.

Gitlin, L., Barchet, W., Gilfillan, S., Cella, M., Beutler, B., Flavell, R.A., Diamond, M.S., and Colonna, M. (2006). Essential role of mda-5 in type I IFN responses to polyriboinosinic:polyribocytidylic acid and encephalomyocarditis picornavirus. Proc. Natl. Acad. Sci. USA *103*, 8459–8464.

Gorbalenya, A.E., Koonin, E.V., Donchenko, A.P., and Blinov, V.M. (1988). A novel superfamily of nucleoside triphosphate-binding motif containing proteins which are probably involved in duplex unwinding in DNA and RNA replication and recombination. FEBS Lett. *235*, 16–24.

Hiscott, J., Lin, R., Nakhaei, P., and Paz, S. (2006). MasterCARD: a priceless link to innate immunity. Trends Mol. Med. *12*, 53–56.

Holm, L., and Sander, C. (1993). Protein structure comparison by alignment of distance matrices. J. Mol. Biol. *233*, 123–138.

Hopfner, K.P., and Tainer, J.A. (2003). Rad50/SMC proteins and ABC transporters: unifying concepts from high-resolution structures. Curr. Opin. Struct. Biol. *13*, 249–255.

Hopfner, K.P., and Michaelis, J. (2007). Mechanisms of nucleic acid translocases: lessons from structural biology and single-molecule biophysics. Curr. Opin. Struct. Biol. *17*, 87–95.

Hornung, V., Ellegast, J., Kim, S., Brzozka, K., Jung, A., Kato, H., Poeck, H., Akira, S., Conzelmann, K.K., Schlee, M., et al. (2006). 5′-triphosphate RNA is the ligand for RIG-I. Science *314*, 994–997.

Itzen, A., Pylypenko, O., Goody, R.S., Alexandrov, K., and Rak, A. (2006). Nucleotide exchange via local protein unfolding—structure of Rab8 in complex with MSS4. EMBO J. *25*, 1445–1455.

Johnson, C.L., and Gale, M., Jr. (2006). CARD games between virus and host get a new player. Trends Immunol. *27*, 1–4.

Kabsch, W. (1993). Automatic processing of rotation diffraction data from crystals of initially unknown symmetry and cell constants. J. Appl. Crystallogr. *21*, 916–924.

Kato, H., Takeuchi, O., Sato, S., Yoneyama, M., Yamamoto, M., Matsui, K., Uematsu, S., Jung, A., Kawai, T., Ishii, K.J., et al. (2006). Differential roles of MDA5 and RIG-I helicases in the recognition of RNA viruses. Nature *441*, 101–105.

Kawai, T., and Akira, S. (2006). Innate immune recognition of viral infection. Nat. Immunol. *7*, 131–137.

Kawai, T., Takahashi, K., Sato, S., Coban, C., Kumar, H., Kato, H., Ishii, K.J., Takeuchi, O., and Akira, S. (2005). IPS-1, an adaptor triggering RIG-I- and Mda5-mediated type I interferon induction. Nat. Immunol. *6*, 981–988.

Komuro, A., and Horvath, C.M. (2006). RNA- and virus-independent inhibition of antiviral signaling by RNA helicase LGP2. J. Virol. *80*, 12332–12342.

Meylan, E., Curran, J., Hofmann, K., Moradpour, D., Binder, M., Bartenschlager, R., and Tschopp, J. (2005). Cardif is an adaptor protein in the RIG-I antiviral pathway and is targeted by hepatitis C virus. Nature *437*, 1167–1172.

Meylan, E., Tschopp, J., and Karin, M. (2006). Intracellular pattern recognition receptors in the host response. Nature *442*, 39–44.

Pichlmair, A., Schulz, O., Tan, C.P., Naslund, T.I., Liljestrom, P., Weber, F., and Reis e Sousa, C. (2006). RIG-I-mediated antiviral responses to single-stranded RNA bearing 5′-phosphates. Science *314*, 997–1001.

Plumet, S., Herschke, F., Bourhis, J.M., Valentin, H., Longhi, S., and Gerlier, D. (2007). Cytosolic 5′-triphosphate ended viral leader transcript of measles virus as activator of the RIG I-mediated interferon response. PLoS ONE *2*, e279. 10.1371/journal.pone.0000279.

Rothenfusser, S., Goutagny, N., DiPerna, G., Gong, M., Monks, B.G., Schoenemeyer, A., Yamamoto, M., Akira, S., and Fitzgerald, K.A. (2005). The RNA helicase Lgp2 inhibits TLR-independent sensing of viral replication by retinoic acid-inducible gene-I. J. Immunol. *175*, 5260–5268.

Saito, T., Hirai, R., Loo, Y.M., Owen, D., Johnson, C.L., Sinha, S.C., Akira, S., Fujita, T., and Gale, M., Jr. (2007). Regulation of innate antiviral defenses through a shared repressor domain in RIG-I and LGP2. Proc. Natl. Acad. Sci. USA *104*, 582–587.

Seth, R.B., Sun, L., Ea, C.K., and Chen, Z.J. (2005). Identification and characterization of MAVS, a mitochondrial antiviral signaling protein that activates NF-kappaB and IRF 3. Cell *122*, 669–682.

Seth, R.B., Sun, L., and Chen, Z.J. (2006). Antiviral innate immunity pathways. Cell Res. *16*, 141–147.

Sumpter, R., Jr., Loo, Y.M., Foy, E., Li, K., Yoneyama, M., Fujita, T., Lemon, S.M., and Gale, M., Jr. (2005). Regulating intracellular antiviral defense and permissiveness to hepatitis C virus RNA replication through a cellular RNA helicase, RIG-I. J. Virol. *79*, 2689–2699.

Xu, L.G., Wang, Y.Y., Han, K.J., Li, L.Y., Zhai, Z., and Shu, H.B. (2005). VISA is an adapter protein required for virus-triggered IFN-beta signaling. Mol. Cell *19*, 727–740.

Yoneyama, M., Kikuchi, M., Natsukawa, T., Shinobu, N., Imaizumi, T., Miyagishi, M., Taira, K., Akira, S., and Fujita, T. (2004). The RNA helicase RIG-I has an essential function in double-stranded RNA-induced innate antiviral responses. Nat. Immunol. *5*, 730–737.

Yoneyama, M., Kikuchi, M., Matsumoto, K., Imaizumi, T., Miyagishi, M., Taira, K., Foy, E., Loo, Y.M., Gale, M., Jr., Akira, S., et al. (2005). Shared and unique functions of the DExD/H-box helicases RIG-I, MDA5, and LGP2 in antiviral innate immunity. J. Immunol. *175*, 2851–2858.

Yu, H., and Schreiber, S.L. (1995). Structure of guanine-nucleotide-exchange factor human Mss4 and identification of its Rab-interacting surface. Nature *376*, 788–791.

Accession Numbers

The Protein Data Bank (PDB) accession number for coordinates and structure factors of zinc-bound RD is 2QFB. The PDB accession number for coordinates and structure factors of mercury-bound RD is 2QFD.

Cell PRESS

Immunity
Minireview

Structural Mechanism of RNA Recognition by the RIG-I-like Receptors

Mitsutoshi Yoneyama[1,2] and Takashi Fujita[1,*]
[1]Laboratory of Molecular Genetics, Institute for Virus Research, and Laboratory of Molecular Cell Biology, Graduate School of Biostudies, Kyoto University, Kyoto, 606-8507, Japan
[2]PRESTO, Japan Science and Technology Agency, 4-1-8 Honcho Kawaguchi, Saitama, Japan
*Correspondence: tfujita@virus.kyoto-u.ac.jp
DOI 10.1016/j.immuni.2008.07.009

Cytoplasmic nonself RNA, such as that generated by invading viruses, is recognized by a family of sensory molecules termed RIG-I-like Receptors (RLRs). Here, we discuss the mechanism of the RLRs' sensing of nonself RNA. Our findings define three functional domains of RLRs and provide insights into how RLRs function as a molecular switch through interactions with virus-specific RNA ligands.

A wide variety of cells in the body are capable of exhibiting antiviral innate immunological responses upon viral infection. Infected viruses are detected by sensory molecules, including Toll-like receptors (TLRs) and RIG-I-like receptors (RLRs: retinoic acid-inducible gene I, RIG-I; melanoma differentiation-associated gene 5, MDA5; and laboratory of genetics and physiology 2, LGP2). Whereas TLRs detect viral components in specific cells, such as dendritic cells and macrophages, RLRs sense the infected viruses in the cytoplasm of most cell types. RLRs sense viral RNA and result in immunological responses, including the production of type I interferon (IFN) and inflammatory cytokines (Akira et al., 2006; Yoneyama et al., 2005; Yoneyama et al., 2004).

Sensing of Specific Viruses by RLRs

Double-stranded (ds) RNA can mimic the induction of the classical antiviral response by being a potent inducer of type I IFN (Samuel, 2001). Analyses of gene-deleted mice and their cells reveal that RIG-I and MDA5 sense specific types of viruses (Gitlin et al., 2006; Kato et al., 2005; Kato et al., 2006): whereas MDA5 senses picornaviruses, RIG-I senses many other viruses, including influenza A, Sendai, vesicular stomatitis, and Japanese encephalitis. This differential recognition is based on the distinct nonself RNA patterns generated by the viruses, as shown by the observation that RIG-I is selectively activated by transfection of in vitro-transcribed RNA, whereas MDA5 is selectively activated by transfection of poly I:C (Kato et al., 2006) (see below). Viral RNA molecules harboring a 5′ppp end, such as in vitro-transcribed RNA, were discovered as a new class of nonself RNA that selectively activates RIG-I (Hornung et al., 2006; Pichlmair et al., 2006). The 5′ppp end of host transcripts (self) is either removed or masked by the attachment of a "cap" before their transport to the cytoplasm. In contrast, although cells infected with influenza virus do not accumulate detectable amounts of dsRNA, viral 5′ppp RNA is produced during infection, leading to the ability of host cells to sense the virus via RIG-I (Pichlmair et al., 2006).

Recognition of the Ligand by the RIG-I ATPase Helicase

Functional analyses revealed that both RIG-I and MDA5 contain an effector domain (CARD: caspase recruitment domain) and a regulatory domain (helicase homology and C-terminal repressor domain) (Saito et al., 2007; Yoneyama et al., 2005; Yoneyama et al., 2004). However, it is not well understood how nonself RNA is physically recognized; for example, neither of these helicases contains a known RNA-binding motif. Recently, a biochemical study using recombinant RIG-I revealed that RIG-I specifically binds to dsRNA, including relatively short (~25 bp) species, or 5′ppp RNA through an interaction with the C-terminal domain (CTD, aa. 792-925) of RIG-I (Takahasi et al., 2008) (see below). Another report demonstrated that a similar C-terminal fragment (aa. 802-925) binds to 5′ppp RNA but not to dsRNA. The reason for this discrepancy is unknown. The failure to detect RIG-I-dsRNA complex may be due to the nonconventional method used (Cui et al., 2008).

As predicted from its primary structure, RIG-I is a ligand-dependent ATPase (Cui et al., 2008; Gee et al., 2008; Takahasi et al., 2008). Mutation of the ATP-binding site (K270A) inactivates RIG-I to trigger antiviral signaling (Yoneyama et al., 2004). However, RIG-I K270A recognizes both dsRNA and 5′ppp RNA (Takahasi et al., 2008). Artificial removal of the CARD rendered it as a constitutive active ATPase (Gee et al., 2008). However, physiological significance of this observation is unknown because excision of the CARD under physiological conditions has not been observed. In vitro helicase assay revealed that the full-length RIG-I selectively unwinds dsRNA harboring 3′-terminal overhang (> 5 nt) in the presence of ATP (Takahasi et al., 2008). Interestingly, although dsRNA resistant to the helicase activity (with either blunt or 5′-terminal overhang end) efficiently induces IFN production in cell culture, those types with 3′-terminal overhang, which are susceptible to being unwound, failed to activate IFN genes. These results indicate that unwinding of dsRNA is not a critical step for triggering signals, as suggested by the observation that single-stranded RNA with a 5′ppp end is a functional ligand for RIG-I. These observations raise the question of what role ATP plays. It is evident that unwinding of dsRNA by RIG-I through ATP hydrolysis does not trigger antiviral signal. Thus, stable formation of a complex between RIG-I and 5′ppp RNA or dsRNA, independent of ATP, may be a prerequisite step for RIG-I activation. If so, the function of ATP is likely the conversion of this precomplex into active conformation through the motor-like function of the DExD/H-box helicase. It remains to

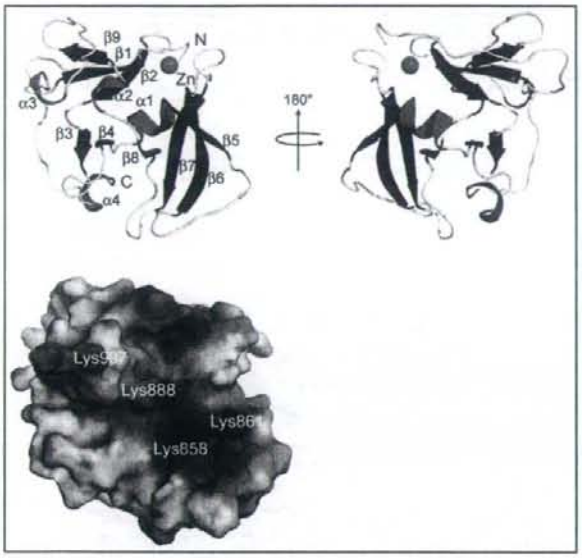

Figure 1. Solution Structure of the RIG-I CTD
Upper panel: ribbon diagram of the RIG-I CTD. The zinc atom, which stabilizes the structure, is indicated as a purple sphere.
Lower panel: Electrostatic surface potential of the RIG-I CTD. One side of the CTD (upper left) displays a cleft lined with basic amino acids (lower). Indicated are the residues critical for dsRNA and 5′ppp-RNA binding and biological activity, as revealed by alanine replacements. (F. Inagaki and K. Takahasi, personal communication).

be shown whether ATP hydrolysis is involved in the conformational change.

RNA-Recognition Domain of RIG-I

Limited protease digestion of the RIG-I-RNA complex revealed that RNA binding induces a digestion-resistant RIG-I fragment (Takahasi et al., 2008). This fragment (aa. 792-925, 17 kD) corresponds to the CTD and is sufficient to recognize dsRNA or 5′ppp RNA. Interestingly, the CTD nearly overlaps with a previously identified repressor domain (aa. 723-925) (Saito et al., 2007). The repressor domain is capable of interacting with the CARD and a helicase domain (helicase linker region, aa. 420-627), and overexpression of the repressor domain blocked RIG-I-mediated signaling; therefore, an autorepression model is proposed, in which the CARD is masked through intramolecular interactions mediated by the repressor domain. The CTD exhibits limited conservation among the RLR family members. However, the repressor function is shared by RIG-I and LGP2.

The atomic structure of the CTD has been determined by nuclear magnetic resonance (NMR) (Takahasi et al., 2008) and X-ray crystallography (Cui et al., 2008), and an essentially identical structure was determined in both crystals and solution. Although the amino acid sequences exhibit little homology to other proteins, the RIG-I CTD is structurally similar to the mammalian suppressor of Sec4 (Mss4), and both structures are stabilized by Zn^{2+} within the molecule (Figure 1). Nevertheless, it is unlikely that RLR and Mss4 are functionally related, because Mss4 is a guanine nucleotide exchange factor and is not known to function as an RNA-binding protein. One side of the CTD exhibits a large cleft with positive surface charges, and the opposite side contains acidic patches. The addition of either dsRNA or 5′ppp RNA specifically titrated the NMR signal of the basic cleft, suggesting that the cleft is an RNA-recognition surface. Consistent with this observation, mutagenesis on the basic cleft specifically reduced both RNA binding and the signaling capacity of RIG-I. In addition, Cui et al. showed via gel-filtration analysis that the RIG-I CTD recognizes 5′ppp RNA as a CTD dimer (Cui et al., 2008). Similarly, recombinant LGP2 binds to dsRNA and forms a large complex (Murali et al., 2008). It is likely that a single dsRNA molecule can simultaneously bind to multiple CTD molecules. Alternatively, it is possible that dsRNA can induce protein-protein association to form a dimer (oligomer), as in the case of TLR3 recognition of dsRNA (Liu et al., 2008); therefore, structural determination of the complex is necessary to address this issue.

Functional studies suggest that the CTD retains two distinct functions: RNA recognition and signal repression. Mutagenesis on the basic concave surface inactivated RNA recognition; however, none of the mutations rendered RIG-I constitutively active, suggesting that RNA-recognition surfaces and RNA-repression surfaces do not overlap. Furthermore, ATP binding or hydrolysis is not required for the recognition of RNA by RIG-I, suggesting a model for inactive RIG-I, as depicted in Figure 2, in which the repressor domain mediates a closed structure through intramolecular interactions but the RNA-binding domain is available. When viruses produce dsRNA or 5′ppp RNA, these types of nonself RNA bind to the concave RNA-recognition surface and induce conformational change in the presence of ATP, then the CARD is exposed. The released CARD forms complexes with either other RIG-I molecules or downstream adaptor Interferon Promoter Stimulator-1 (IPS-1, also known as MAVS, VISA, and Cardif) to transduce biological signals.

Long versus Short dsRNA

As mentioned above, RIG-I and MDA5 differentially recognize nonself RNA. However, the underlying mechanism of this recognition is not clear. Although the CTDs of both RIG-I and MDA5 share common residues, their surface charges diverged (our unpublished observation). Poly I:C is the only defined synthetic RNA ligand for MDA5. Commercial poly I:C is made by annealing poly I and poly C with 5′pp (approximately 1000 bases or longer). Although commercial poly I:C (> 3 kbp) selectively activates MDA5, short poly I:C generated by enzyme digestion (~300 bp) is unable to activate MDA5 but acts as a potent ligand for RIG-I (Kato et al., 2008). In vitro assay using recombinant RIG-I and MDA5 also showed that short and long poly I:C preferentially induced ATPase activity for RIG-I and MDA5, respectively. Consistent with these observations, short dsRNA species (1.2~1.4 kbp) of the Reovirus genome selectively activated RIG-I but longer dsRNA (3.4 kbp) was capable of activating MDA5. These results strongly suggest that RIG-I and MDA5 discriminate long and short dsRNA (Figure 3); however, the mechanism underlying the sensing of nucleotide length is unknown.

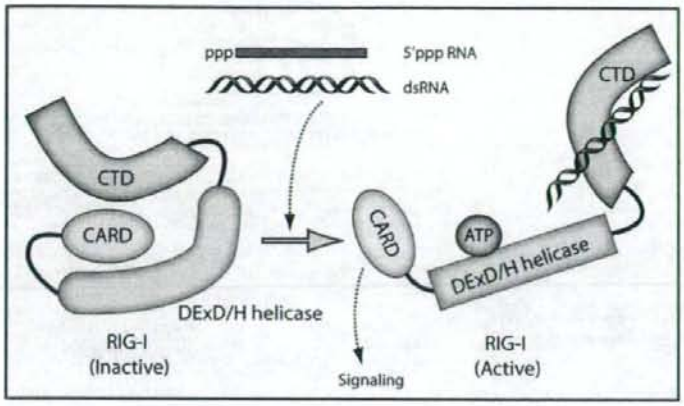

Figure 2. Model of RIG-I Activation by Nonself RNA
The CTD coincides with the functionally defined repressor domain and interacts with both the helicase domain and the CARD in the absence of its ligand. When viruses produce dsRNA or 5'ppp-RNA, these types of nonself RNA bind to the RNA-recognition cleft on the CTD and induce conformational change in the presence of ATP, then the CARD is exposed. The released CARD forms complexes with either other RIG-I molecules or downstream adaptor IPS-1 to transduce biological signals.

Why long poly I:C does not activate RIG-I despite its high affinity to poly I:C, particularly in MDA5 deficient cells, is unclear. One clue is the observation that although short dsRNA and 5'ppp RNA induce protease-resistant 30 kD and 17 kD fragments of RIG-I, poly I:C induces a 60 kD fragment (Takahasi et al., 2008). This result suggests that poly I:C binds to RIG-I but induces an abortive conformation of RIG-I, rendering it incapable of signaling downstream. Evidently, this issue requires further structural analyses.

Viral Strategy for Evading Host Recognition

Different viruses produce distinct classes of RNA patterns in infected cells. So far, three types of RNA patterns that can be recognized by host cells have been identified: 5'ppp RNA, short dsRNA, and long dsRNA. Naturally, viruses try to avoid detection from host antiviral mechanisms, and they have developed various strategies for escaping detection. As reported recently, several negative-strand RNA viruses, including Hantaan virus, Crimean-Congo hemorrhagic fever virus, and Borna disease virus, manage to cleave off the 5'ppp structure of viral genomic RNA (Habjan et al., 2008) (Figure 3). In addition, picornaviruses covalently link VPg protein at the 5' end of viral RNA by disrupting the 5'ppp structure (Paul, 2002). Picornaviruses also accumulate long replicative form (RF) dsRNA in infected cells, which may block the function of RIG-I. However, MDA5, with its ability to sense longer dsRNA, may provide a secondary checkpoint to counter this viral hiding strategy. In addition, viruses encode protein inhibitors, such as nonstructural (NS) proteins NS1 (influenza), NS3/4A (hepatitis C), V (paramyxoviruses), and VP35 (ebola) that disrupt the antiviral-signaling cascade (Yoneyama and Fujita, 2007), and these could work in concert to block the host antiviral response. These results highlight the offense and defense between host mechanism of nonself RNA detection and viral evolution.

Conclusion and Future Perspective

The understanding of how foreign RNA species are recognized by RLRs has advanced substantially. It is now evident that in addition to the DExD/H helicase domain, the CTD and the CARD, which sense foreign RNA and execute signaling, respectively, are essential for RIG-I function. The current model suggests that these domains may interact with each other and that ligand RNA interaction may induce critical conformational changes to trigger biological signals. In this regard, it will be important to determine the structure of full-length RIG-I at the atomic level with

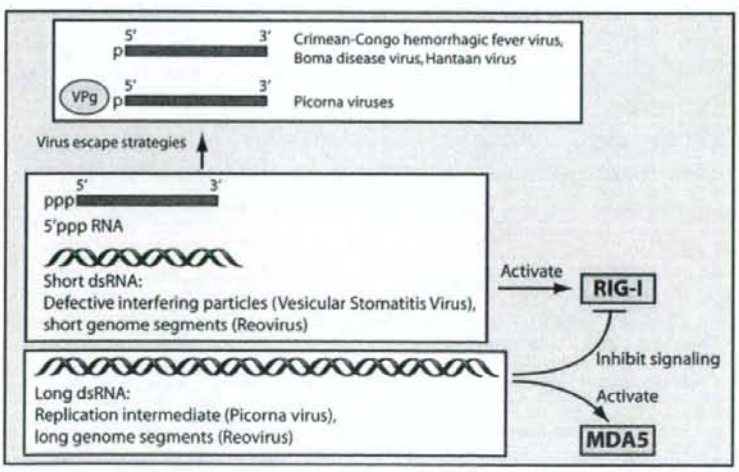

Figure 3. Nonself-RNA-Recognition Specificity of RIG-I and MDA5
5'ppp RNA and short dsRNA are specifically recognized by RIG-I. Although long dsRNA may block RIG-I for signaling, it efficiently activates MDA5. Some viruses are known to modify viral 5'ppp residues to escape detection by RIG-I.

and without its ligand in order to finalize our understanding of this process. Furthermore, this will provide clues for understanding functions of other, numerous DExD/H helicases.

ACKNOWLEDGMENTS

We thank F. Inagaki and K. Takahasi for provision of the NMR structure of the RIG-I CTD.

REFERENCES

Akira, S., Uematsu, S., and Takeuchi, O. (2006). Pathogen recognition and innate immunity. Cell *124*, 783–801.

Cui, S., Eisenacher, K., Kirchhofer, A., Brzozka, K., Lammens, A., Lammens, K., Fujita, T., Conzelmann, K.K., Krug, A., and Hopfner, K.P. (2008). The C-terminal regulatory domain is the RNA 5′-triphosphate sensor of RIG-I. Mol. Cell *29*, 169–179.

Gee, P., Chua, P.K., Gevorkyan, J., Klumpp, K., Najera, I., Swinney, D.C., and Deval, J. (2008). Essential role of the N-terminal domain in the regulation of RIG-I ATPase activity. J. Biol. Chem. *283*, 9488–9496.

Gitlin, L., Barchet, W., Gilfillan, S., Cella, M., Beutler, B., Flavell, R.A., Diamond, M.S., and Colonna, M. (2006). Essential role of mda-5 in type I IFN responses to polyriboinosinic:polyribocytidylic acid and encephalomyocarditis picornavirus. Proc. Natl. Acad. Sci. USA *103*, 8459–8464.

Habjan, M., Andersson, I., Klingstrom, J., Schumann, M., Martin, A., Zimmermann, P., Wagner, V., Pichlmair, A., Schneider, U., Muhlberger, E., et al. (2008). Processing of genome 5′ termini as a strategy of negative-strand RNA viruses to avoid RIG-I-dependent interferon induction. PLoS ONE *3*, e2032.

Hornung, V., Ellegast, J., Kim, S., Brzozka, K., Jung, A., Kato, H., Poeck, H., Akira, S., Conzelmann, K.K., Schlee, M., et al. (2006). 5′-Triphosphate RNA is the ligand for RIG-I. Science *314*, 994–997.

Kato, H., Sato, S., Yoneyama, M., Yamamoto, M., Uematsu, S., Matsui, K., Tsujimura, T., Takeda, K., Fujita, T., Takeuchi, O., and Akira, S. (2005). Cell type-specific involvement of RIG-I in antiviral response. Immunity *23*, 19–28.

Kato, H., Takeuchi, O., Mikano-Satoh, E., Hirai, R., Kawai, T., Matsushita, K., Hiiragi, A., Dermody, T., Fujita, T., and Akira, S. (2008). The length-dependent recognition of double-stranded RNAs by RIG-I and MDA5. J. Exp. Med. *205*, 1601–1610.

Kato, H., Takeuchi, O., Sato, S., Yoneyama, M., Yamamoto, M., Matsui, K., Uematsu, S., Jung, A., Kawai, T., Ishii, K.J., et al. (2006). Differential roles of MDA5 and RIG-I helicases in the recognition of RNA viruses. Nature *441*, 101–105.

Liu, L., Botos, I., Wang, Y., Leonard, J.N., Shiloach, J., Segal, D.M., and Davies, D.R. (2008). Structural basis of toll-like receptor 3 signaling with double-stranded RNA. Science *320*, 379–381.

Murali, A., Li, X., Ranjith-Kumar, C.T., Bhardwaj, K., Holzenburg, A., Li, P., and Kao, C.C. (2008). Structure and Function of LGP2, a DEX(D/H) Helicase That Regulates the Innate Immunity Response. J. Biol. Chem. *283*, 15825–15833.

Paul, A.V. (2002). Possible unifying mechanism of Picornavirus genome replication. In Molecular Biology of Picornaviruses, B. Selmler and E. Wimmer, eds. (Washington, DC: ASM Press), pp. 227–246.

Pichlmair, A., Schulz, O., Tan, C.P., Naslund, T.I., Liljestrom, P., Weber, F., and Reis e Sousa, C. (2006). RIG-I-mediated antiviral responses to single-stranded RNA bearing 5′-phosphates. Science *314*, 997–1001.

Saito, T., Hirai, R., Loo, Y.M., Owen, D., Johnson, C.L., Sinha, S.C., Akira, S., Fujita, T., and Gale, M., Jr. (2007). Regulation of innate antiviral defenses through a shared repressor domain in RIG-I and LGP2. Proc. Natl. Acad. Sci. USA *104*, 582–587.

Samuel, C.E. (2001). Antiviral actions of interferons. Clin. Microbiol. Rev. *14*, 778–809.

Takahasi, K., Yoneyama, M., Nishihori, T., Hirai, R., Kumeta, H., Narita, R., Gale, M., Jr., Inagaki, F., and Fujita, T. (2008). Nonself RNA-sensing mechanism of RIG-I helicase and activation of antiviral immune responses. Mol. Cell *29*, 428–440.

Yoneyama, M., and Fujita, T. (2007). Function of RIG-I-like receptors in antiviral innate immunity. J. Biol. Chem. *282*, 15315–15318.

Yoneyama, M., Kikuchi, M., Matsumoto, K., Imaizumi, T., Miyagishi, M., Taira, K., Foy, E., Loo, Y.M., Gale, M., Jr., Akira, S., et al. (2005). Shared and Unique Functions of the DExD/H-Box Helicases RIG-I, MDA5, and LGP2 in Antiviral Innate Immunity. J. Immunol. *175*, 2851–2858.

Yoneyama, M., Kikuchi, M., Natsukawa, T., Shinobu, N., Imaizumi, T., Miyagishi, M., Taira, K., Akira, S., and Fujita, T. (2004). The RNA helicase RIG-I has an essential function in double-stranded RNA-induced innate antiviral responses. Nat. Immunol. *5*, 730–737.

JOURNAL OF VIROLOGY, Oct. 2008, p. 9639–9646
0022-538X/08/$08.00+0 doi:10.1128/JVI.00351-08

Vol. 82, No. 19

The DNA Damage Sensors Ataxia-Telangiectasia Mutated Kinase and Checkpoint Kinase 2 Are Required for Hepatitis C Virus RNA Replication▽

Yasuo Ariumi,[1] Misao Kuroki,[1] Hiromichi Dansako,[1] Ken-Ichi Abe,[1] Masanori Ikeda,[1] Takaji Wakita,[2] and Nobuyuki Kato[1]*

Department of Molecular Biology, Okayama University Graduate School of Medicine, Dentistry, and Pharmaceutical Sciences, 2-5-1, Shikata-cho, Okayama 700-8558, Japan,[1] and Department of Virology II, National Institute of Infectious Diseases, 1-23-1 Toyama, Shinjuku-ku, Tokyo 162-8640, Japan[2]

Received 18 February 2008/Accepted 18 July 2008

Cellular responses to DNA damage are crucial for maintaining genome integrity, virus infection, and preventing the development of cancer. Hepatitis C virus (HCV) infection and the expression of the HCV nonstructural protein NS3 and core protein have been proposed as factors involved in the induction of double-stranded DNA breaks and enhancement of the mutation frequency of cellular genes. Since DNA damage sensors, such as the ataxia-telangiectasia mutated kinase (ATM), ATM- and Rad3-related kinase (ATR), poly(ADP-ribose) polymerase 1 (PARP-1), and checkpoint kinase 2 (Chk2), play central roles in the response to genotoxic stress, we hypothesized that these sensors might affect HCV replication. To test this hypothesis, we examined the level of HCV RNA in HuH-7-derived cells stably expressing short hairpin RNA targeted to ATM, ATR, PARP-1, or Chk2. Consequently, we found that replication of both genome-length HCV RNA (HCV-O, genotype 1b) and the subgenomic replicon RNA were notably suppressed in ATM- or Chk2-knockdown cells. In addition, the RNA replication of HCV-JFH1 (genotype 2a) and the release of core protein into the culture supernatants were suppressed in these knockdown cells after inoculation of the cell culture-generated HCV. Consistent with these observations, ATM kinase inhibitor could suppress the HCV RNA replication. Furthermore, we observed that HCV NS3-NS4A interacted with ATM and that HCV NS5B interacted with both ATM and Chk2. Taken together, these results suggest that the ATM signaling pathway is critical for HCV RNA replication and may represent a novel target for the clinical treatment of patients with chronic hepatitis C.

Hepatitis C virus (HCV) infection frequently causes chronic hepatitis, which progresses to liver cirrhosis and hepatocellular carcinoma. HCV infection has now become a serious health problem, with at least 170 million people currently infected worldwide (28). HCV is an enveloped virus with a positive single-stranded 9.6-kb RNA genome, which encodes a large polyprotein precursor of approximately 3,000 amino acid residues. This polyprotein is cleaved by a combination of the host and viral proteases into at least 10 proteins in the following order: core, envelope 1 (E1), E2, p7, nonstructural 2 (NS2), NS3, NS4A, NS4B, NS5A, and NS5B (12, 13, 27).

Studies have shown that various viruses with distinct replication strategies—including the DNA viruses Epstein-Barr virus, herpes simplex virus 1, adenovirus, and simian virus 40 and the retrovirus human immunodeficiency virus type 1 (HIV-1)—can activate DNA damage response pathways and utilize these damage responses to facilitate their own viral reproduction and promote the survival of infected cells (2, 16, 17). In the case of HCV, it has been proposed that HCV infection causes double-stranded DNA (dsDNA) breaks and enhances the mutation frequency of cellular genes and that these effects are mediated by nitric oxide (18, 19). In addition, the HCV core, E1, and NS3 proteins have been suggested to be potent reactive oxygen species inducers, leading to DNA damage (19). Furthermore, we previously demonstrated that HCV NS5B-expressing PH5CH8 immortalized human hepatocyte cells were susceptible to DNA damage in the form of dsDNA breaks (23). Thus, HCV seems to be associated with the dsDNA damage response pathways.

Since the DNA damage sensors, such as ataxia-telangiectasia mutated kinase (ATM), ATM- and Rad3-related kinase (ATR), poly(ADP-ribose) polymerase 1 (PARP-1), and checkpoint kinase 2 (Chk2; a direct downstream target of ATM), play central roles in response to genotoxic stress (10), we hypothesized that these sensors might affect HCV replication.

To investigate the possible involvement of these cellular factors in HCV replication, we examined the level of HCV RNA in cells rendered defective for DNA damage sensors by RNA interference or by pharmacological inhibition.

MATERIALS AND METHODS

Cell culture. 293FT cells were cultured in Dulbecco's modified Eagle's medium (DMEM; Invitrogen, Carlsbad, CA) supplemented with 10% fetal bovine serum (FBS). The HuH-7-derived O cells harboring a replicative genome-length HCV RNA and the HuH-7-derived sO cells harboring the subgenomic replicon RNA of HCV-O were cultured in DMEM with 10% FBS and G418 (300 μg/ml geneticin; Invitrogen) as described previously (11, 14). Oc and sOc cells, which were created by eliminating HCV RNA from O cells and sO cells by interferon (IFN) treatment (11, 14), respectively, were also cultured in DMEM with 10% FBS.

RNA interference. Oligonucleotides with the following sense and antisense sequences were used for the cloning of short hairpin RNA (shRNA)-encoding se-

* Corresponding author. Mailing address: Department of Molecular Biology, Okayama University Graduate School of Medicine, Dentistry, and Pharmaceutical Sciences, 2-5-1, Shikata-cho, Okayama 700-8558, Japan. Phone: 81 86 235 7385. Fax: 81 86 235 7392. E-mail: nkato@md.okayama-u.ac.jp.

▽ Published ahead of print on 30 July 2008.

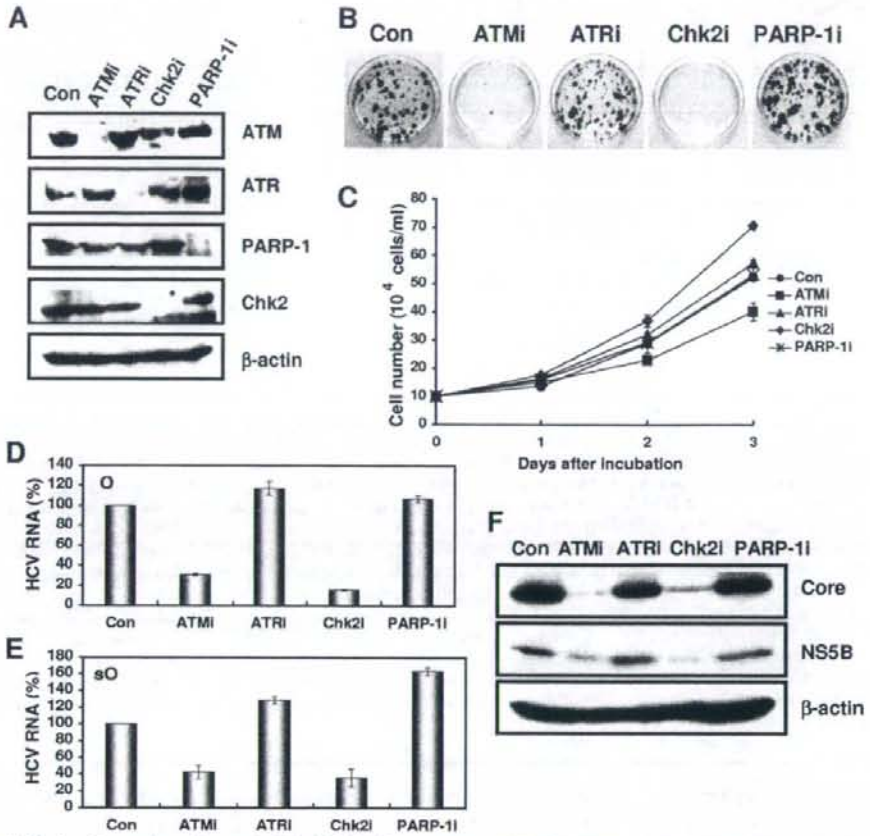

FIG. 1. The ATM signaling pathway is required for HCV RNA replication. (A) Inhibition of ATM, ATR, Chk2, or PARP-1 expression by shRNA-producing lentiviral vectors. The results of the Western blot analysis of cellular lysates with anti-ATM, anti-ATR, anti-Chk2, anti-PARP-1, or anti-β-actin antibody in Oc cells expressing shRNA targeted to ATM (ATMi), ATR (ATRi), Chk2 (Chk2i), or PARP-1 (PARP-1i) as well as in Oc cells transduced with a control lentiviral vector (Con) are shown. (B) ECF in ATM-, ATR-, Chk2-, or PARP-1-knockdown cells. In vitro transcribed ON/C-5B K1609E RNA (2 μg) was transfected into the ATM-, ATR-, Chk2, or PARP-1-knockdown Oc cells or the Oc cells transduced with a control lentiviral vector (Con). G418-resistant colonies were stained with Coomassie brilliant blue at 3 weeks after electroporation of RNA. Experiments were done in duplicate, and a representative result is shown. (C) The cell growth curve of ATM (ATMi), ATR (ATRi), Chk2 (Chk2i), or PARP-1 (PARP-1i)-knockdown Oc cells or the Oc cells transduced with a control lentiviral vector (Con). Results from three independent experiments are shown. (D) The level of genome-length HCV-O RNA was monitored by real-time LightCycler PCR (Roche). Experiments were done in triplicate, and columns represent the mean percentage of HCV RNA. (E) The level of subgenomic replicon (sO cells) RNA was monitored by real-time LightCycler PCR. Results from three independent experiments are shown as described in panel D. (F) The HCV core or NS5B protein expression level in ATM-, ATR-, Chk2-, or PARP-1-knockdown cells. The results of Western blot analysis of cellular lysates with anti-HCV core protein, anti-HCV NS5B, or anti-β-actin antibody in O cells expressing shRNA targeted to ATM (ATMi), ATR (ATRi), Chk2 (Chk2i), or PARP-1 (PARP-1i) as well as in O cells transduced with a control lentiviral vector (Con) are shown.

quences targeted to Chk2 in lentiviral vector: 5'-GATCCCCGGGGGAGAGCTGTT TGACATTCAAGAGATGTCAAACAGCTCTCCCCCTTTTTGGAAA-3' (sense) and 5'-AGCTTTTCCAAAAAGGGGGAGAGCTGTTTGACATCTCTTGAATGT CAAACAGCTCTCCCCCGGG-3' (antisense). The oligonucleotides above were annealed and subcloned into the BglII-HindIII site, downstream from an RNA polymerase III promoter of pSUPER (5), generating pSUPER-Chk2i. To construct pLV-Chk2i, the BamHI-SalI fragments of the pSUPER-Chk2i were subcloned into the BamHI-SalI site of pRDI292, an HIV-1-derived self-inactivating lentiviral vector containing a puromycin resistance marker allowing for the selection of transduced cells (4). pLV-ATMi, pLV-ATRi, and pLV-PARP-1i were constructed as described previously (1).

Lentiviral vector production. The vesicular stomatitis virus G protein (VSV-G)-pseudotyped HIV-1-based vector system has been described previously (24). The lentiviral vector particles were produced by transient transfection of the second-generation packaging construct pCMV-ΔR8.91 (30) and the VSV-G envelope plasmid pMDG2 as well as the lentiviral vector into 293FT cells with FuGene6 (Roche Diagnostics, Mannheim, Germany).

Quantitative reverse transcription-PCR analysis. Quantitative reverse transcription-PCR analysis for HCV RNA was performed by real-time LightCycler PCR as described previously (11).

Western blot analysis. Cells were lysed in buffer containing 50 mM Tris-HCl (pH 8.0), 150 mM NaCl, 4 mM EDTA, 1% Nonidet P-40, 0.1% sodium dodecyl sulfate (SDS), 1 mM dithiothreitol, and 1 mM phenylmethylsulfonyl fluoride. Supernatants from these lysates were subjected to SDS-polyacrylamide gel electrophoresis, followed by immunoblotting analysis using anti-ATM (2C1; GTX70103 [GeneTex, San Antonio, TX]), anti-ATR (GTX70133; GeneTex), anti-Chk2 (NT; ProSci, Poway, CA), anti-Chk2 (DCS-273; Medical and Biological Laboratories, Nagoya, Japan), anti-phospho-Chk2 (Thr68) (Cell Signaling,

Danvers, MA), anti-PARP-1 (C-2-10; Calbiochem, Merck Biosciences, Darmstadt, Germany), anti-hemagglutinin (HA) (HA-7; Sigma, St. Louis, MO), anti-core protein (CP-9 and CP-11; Institute of Immunology, Tokyo, Japan), anti-NS3 and anti-NS5B (no. 14; a generous gift from M. Kohara, the Tokyo Metropolitan Institute of Medical Science, Japan), anti-NS5A (no. 8926; a generous gift from A. Takamizawa, The Research Foundation for Microbial Diseases of Osaka University, Japan), and anti-β-actin (Sigma) Antibodies.

Immunofluorescence and confocal microscopic analysis. Cells were fixed in 3.5% formaldehyde in phosphate-buffered saline (PBS) and permeabilized in 0.1% NP-40 in PBS at room temperature. Cells were incubated with anti-ATM antibody (5C2; GTX70107 [GeneTex] or PM026 [MBL]), anti-HA antibody (3F10), anti-NS5B antibody and/or anti-NS3 antibody at a 1:300 dilution in PBS containing 3% bovine serum albumin at 37°C for 30 min. Cells were then stained with fluorescein isothiocyanate (FITC)-conjugated anti-rabbit antibody (Jackson ImmunoResearch, West Grove, PA) or anti-Cy3-conjugated anti-mouse antibody (Jackson ImmunoResearch) at a 1:300 dilution in PBS containing bovine serum albumin at 37°C for 30 min. Following extensive washing in PBS, cells were mounted on slides using a mounting medium of 90% glycerin–10% PBS with 0.01% *p*-phenylenediamine added to reduce fading. Samples were viewed under a confocal laser-scanning microscope (LSM510; Zeiss, Jena, Germany).

Immunoprecipitation. Cells were lysed in buffer containing 10 mM Tris-HCl (pH 8.0), 150 mM NaCl, 4 mM EDTA, 0.5% NP-40, 10 mM NaF, 1 mM dithiothreitol, and 1 mM phenylmethylsulfonyl fluoride. Lysates were precleared with 30 μl of protein G-Sepharose (GE Healthcare Biosciences, Uppsala, Sweden). Precleared supernatants were incubated with 5 μg of anti-HA antibody (3F10; Roche), 10 μl of anti-NS5B antibody, 5 μg of anti-Chk2 antibody (DCS-273; MBL), 5 μg of anti-FLAG antibody (M2; Sigma), or 5 μg of anti-ATM antibody (2C1) (GTX70103; GeneTex) at 4°C for 1 h. Following absorption of the precipitates on 30 μl of protein G-Sepharose resin for 1 h, the resin was washed four times with 700 μl of lysis buffer. Proteins were eluted by boiling the resin for 5 min in 2× Laemmli sample buffer. The proteins were then subjected to SDS-polyacrylamide gel electrophoresis, followed by immunoblotting analysis using anti-ATM, anti-Chk2, anti-HCV core protein (CP-9 and CP-11 mixture), anti-NS5A, anti-NS5B, anti-HA (HA-7; Sigma), or anti-NS3 antibody.

RESULTS

ATM and Chk2 are required for HCV RNA replication. To determine the potential role of DNA damage sensors in HCV replication, we first used lentiviral vector-mediated RNA interference to stably knockdown ATM, ATR, PARP-1 (1), or Chk2 in the following human hepatoma HuH-7-derived cell lines: O cells harboring a replicative genome-length HCV RNA (HCV-O, genotype 1b) (11), Oc cells derived from O cells (created by eliminating genome-length HCV RNA from O cells by IFN treatment) (11), sO cells harboring the subgenomic replicon of HCV-O (14), or RSc cells that cell culture-generated HCV (HCVcc) (JFH1, genotype 2a) (29) could infect and effectively replicate (3). To express shRNAs targeted to ATM, ATR, PARP-1 (1), or Chk2, we used a VSV-G-pseudotyped HIV-1-based vector system (24). We used puromycin-resistant pooled cells 10 days after the lentiviral transduction in all experiments. Western blot analysis of the lysates demonstrated very effective knockdown of ATM, ATR, Chk2, and PARP-1 in Oc cells (Fig. 1A). The effective knockdown of ATM, ATR, Chk2, or PARP-1 in O cells or sO cells was also confirmed by Western blot analysis (data not shown). In this context, the efficiency of colony formation (ECF) in ATM- or Chk2-, but not ATR- or PARP-1-, knockdown Oc cells transfected with the genome-length HCV-O RNA with an adapted mutation at amino acid position 1609 in the NS3 helicase region (ON/C-5B K1609E RNA) (11) was notably reduced compared with the control cells (Fig. 1B) even though Chk2-knockdown cells had a slightly faster growth rate than the control cells (Fig. 1C), suggesting that both ATM and Chk2 are crucial for HCV RNA replication. To further confirm this

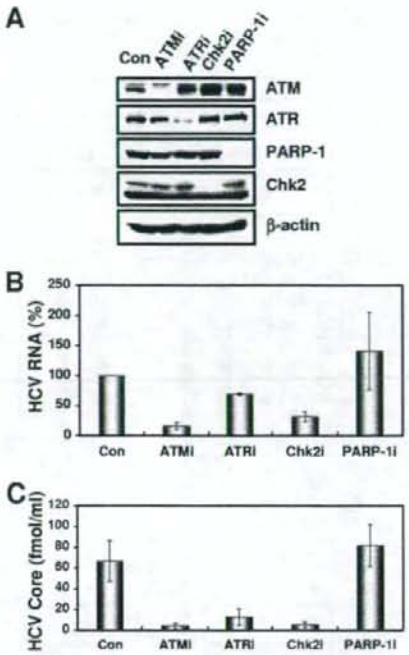

FIG. 2. ATM affects HCV infection. (A) Inhibition of ATM, ATR, Chk2, or PARP-1 expression by shRNA-producing lentiviral vectors. The results of Western blot analysis of cellular lysates with anti-ATM, anti-ATR, anti-PARP-1, anti-Chk2, or anti-β-actin antibody in RSc cured cells expressing shRNA targeted to ATM (ATMi), ATR (ATRi), Chk2 (Chk2i), or PARP-1 (PARP-1i) as well as in RSc cells transduced with a control lentiviral vector (Con) are shown. (B) The level of genome-length HCV (JFH1) RNA was monitored by real-time LightCycler PCR after inoculation of the HCVcc. Results from three independent experiments are shown as described in the legend of Fig. 1D. (C) The levels of the core protein in the culture supernatants were determined by enzyme-linked immunosorbent assay (Mitsubishi Kagaku Bio-Clinical Laboratories). Experiments were done in triplicate, and columns represent the mean core protein levels.

observation, we quantitatively examined the level of HCV RNA in the O cell- or sO cell-derived knockdown cells. Consequently, we found that replication of both genome-length HCV RNA (HCV-O) and its subgenomic replicon RNA (sO) were notably suppressed in ATM- or Chk2-knockdown cells but not in ATR- or PARP-1-knockdown cells (Fig. 1D and E). Consistent with this finding, the expression levels of core and NS5B proteins were also significantly decreased in the cell lysates of ATM- or Chk2-knockdown O cells (Fig. 1F). We next examined the replication level of HCV-JFH1 in ATM-, ATR-, Chk2-, or PARP-1-knockdown RSc cells (Fig. 2A). The results revealed that RNA replication of HCV-JFH1 and release of core protein into the culture supernatants were suppressed in only ATM- or Chk2-knockdown RSc cells after inoculation with HCVcc (Fig. 2B and C). Interestingly, the release of core protein into the culture supernatant was also significantly suppressed in ATR-knockdown RSc cells, while HCV RNA replication was slightly suppressed in these cells

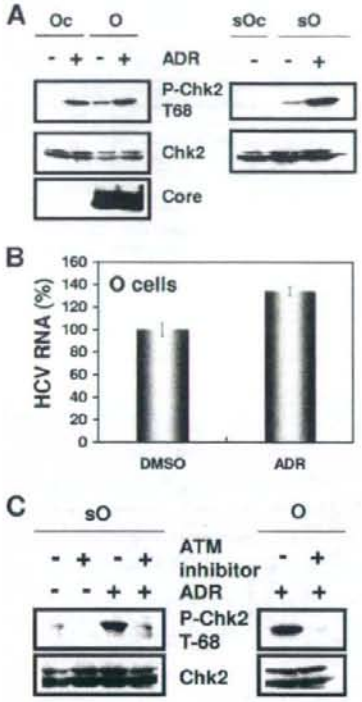

FIG. 3. ATM-dependent DNA damage response in HCV RNA-replicating cells. (A) Stimulation of Chk2 phosphorylation in the HCV RNA-replicating cells. The Oc, O, or sO cells were treated with 100 nM adriamycin (Sigma) for 2 h. The results of Western blot analysis of cellular lysates with anti-phospho-Chk2 (Thr68) (P-Chk2 T68), anti-Chk2, or anti-core protein antibody are shown. (B) Effect of adriamycin on HCV RNA replication. The O cells were treated with 100 nM adriamycin for 24 h. The level of genome-length HCV-O RNA was monitored by real-time LightCycler PCR. Results from three independent experiments are shown as described in the legend of Fig. 1D. DMSO, dimethyl sulfoxide. (C) Effect of ATM kinase inhibitor on Chk2 phosphorylation. The sO or O cells were pretreated with 10 μM ATM kinase inhibitor (KU-55933) (Calbiochem) for 2 h, followed by treatment with 100 nM adriamycin for 2 h. The results of Western blot analysis of cellular lysates with anti-phospho-Chk2 (Thr68) or anti-Chk2 antibody are shown.

(Fig. 2B and C), suggesting that ATR participates in the production of HCV virion.

In contrast, highly efficient knockdown of PARP-1 had no observable effects on the ECF (Fig. 1B), HCV RNA replication (Fig. 1D and E and 2B), or core protein expression in the cell lysate or in the supernatant (Fig. 1F and 2C), suggesting that our finding was not due to a nonspecific event. Thus, we have demonstrated for the first time that DNA damage sensors, ATM and Chk2, are required for HCV RNA replication.

ATM kinase activity in HCV RNA-replicating cells. Although it has been proposed that HCV causes dsDNA breaks (18, 19), little is known about whether HCV activates or inhibits the ATM-dependent damage response pathway. In this regard, it is worth noting that we observed weak but significant Chk2 phosphorylation at threonine 68, the specific marker for

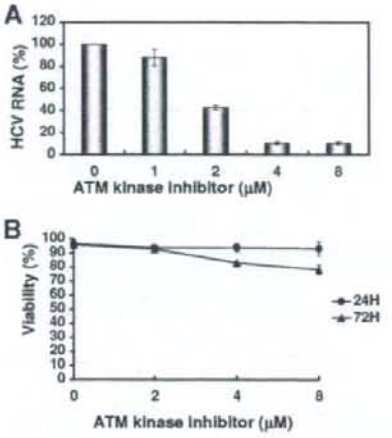

FIG. 4. Suppression of HCV RNA replication by ATM kinase inhibitor. (A) The level of genome-length HCV-O RNA was monitored by real-time LightCycler PCR after treatment with the indicated concentration of ATM kinase inhibitor for 72 h. Results from three independent experiments are shown as described in the legend of Fig. 1D. (B) Cell viabilities after treatment with the indicated concentration of ATM kinase inhibitor for 24 h or 72 h are shown.

ATM activation (20, 21), in the HCV RNA-replicating cells (O and sO cells) but not in the HCV-negative Oc and sOc cells (created by eliminating replicon RNA from sO cells by IFN treatment) (Fig. 3A), suggesting that the persistent HCV RNA replication stimulated the ATM-dependent DNA damage response. Furthermore, a 2-h treatment with 100 nM adriamycin, a dsDNA break inducer, markedly induced Chk2 phosphorylation in Oc, O, and sO cells (Fig. 3A). Importantly, Chk2 phosphorylation was not inhibited even in the HCV RNA-replicating cells (O and sO cells) (Fig. 3A), suggesting that the persistent HCV RNA replication and the HCV proteins are not able to suppress the ATM-dependent DNA damage response. To examine whether such a DNA damage response activates HCV RNA replication, we quantified the level of HCV RNA in the O cells treated with 100 nM adriamycin for 24 h. The results show that HCV RNA replication was increased (approximately 1.3-fold) after treatment with adriamycin (Fig. 3B), suggesting that the DNA damage response activates HCV RNA replication.

Suppression of HCV RNA replication by a small-molecule inhibitor of the ATM kinase. We next examined the effect of a specific small-molecule inhibitor of the ATM kinase (2-morpholin-4-yl-6-thianthren-1-yl-pyran-4-one [KU-55933]) (16) on HCV RNA replication. As expected, the ATM kinase inhibitor effectively inhibited Chk2 phosphorylation after adriamycin treatment in both sO and O cells (Fig. 3C). In this context, the ATM kinase inhibitor could efficiently suppress genome-length HCV RNA replication with an in vitro 50% effective concentration (EC_{50}) of approximately 2 μM at 72 h after treatment with adriamycin (Fig. 4A). Although this ATM kinase inhibitor did not affect cell viability at 24 h after the treatment, there was a slight decrease in the cell viability at 72 h after treatment (Fig. 4B). Thus, this or other ATM kinase inhibitors may be

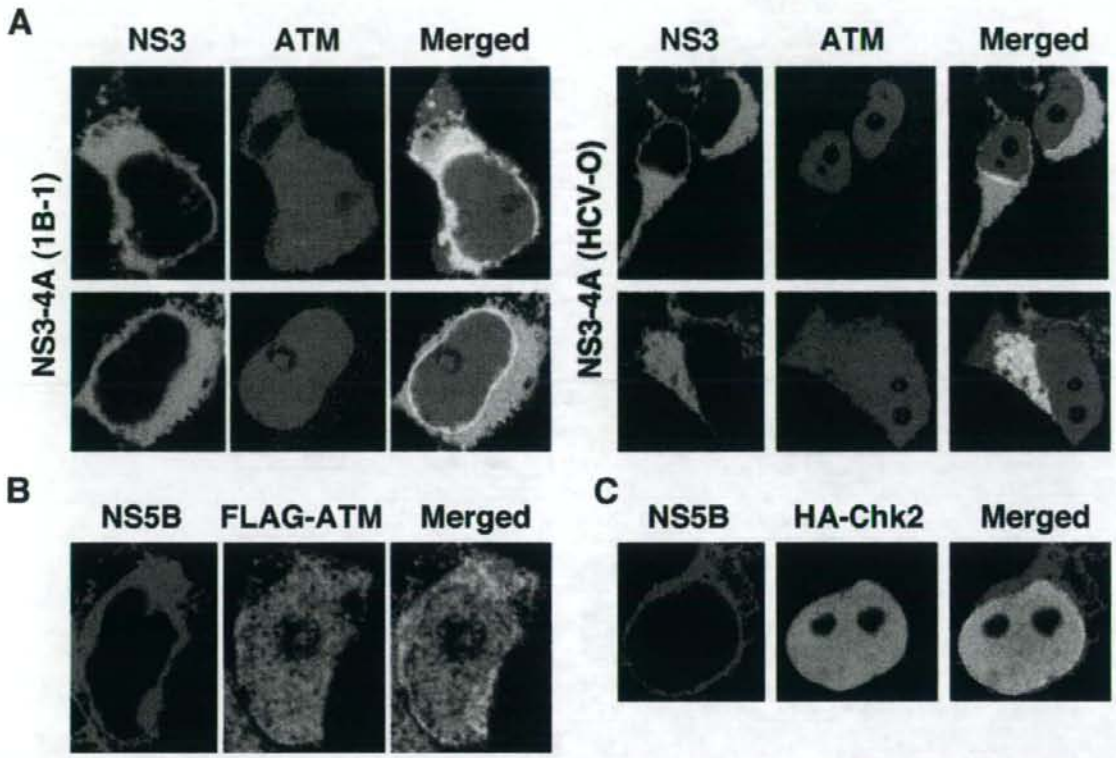

FIG. 5. Subcellular localization of ATM and Chk2 in HCV NS3-4A- or NS5B-expressing cells. (A) ATM partially colocalized with HCV NS3-4A. 293FT cells cotransfected with 300 ng of pCX4bsr/NS3-4A (1B-1) (8) or pCX4bsr/NS3-4A (O) (8) and 300 ng of pcDNA3-FLAG-ATMwt (6) were examined by confocal laser scanning microscopy. Cells were stained with anti-NS3 and anti-ATM (5C2) antibodies and then visualized with FITC (NS3) or Cy3 (ATM). (B) ATM partially colocalized with HCV NS5B. 293FT cells cotransfected with 300 ng of pCX4bsr/NS5B (1B-1) (23) and 300 ng of pcDNA3-FLAG-ATMwt (6). Cells were stained with anti-NS5B (no. 14) and anti-ATM (PM026) antibodies and then visualized with FITC (ATM) or Cy3 (NS5B). (C) Chk2 partially colocalized with HCV NS5B. 293FT cells cotransfected with 300 ng of pCX4bsr/NS5B (1B-1) (23) and 300 ng of pcDNA3-HA-Chk2wt (20, 21). Cells were stained with anti-NS5B and anti-HA (3F10) antibodies and then visualized with FITC (HA-Chk2) or Cy3 (NS5B). Images were visualized using confocal laser scanning microscopy (LSM510; Carl Zeiss). The right panels exhibit two-color overlay images (Merged). Colocalization is shown in yellow.

useful for the clinical treatment of patients with chronic hepatitis C.

Interaction of HCV NS3-4A with ATM. Since HCV NS3 has been proposed to be a viral factor involved in the induction of dsDNA breaks (18, 19), we first examined the subcellular localization of NS3-NS4A ([NS3-4A] 1B-1 or HCV-O strain) and ATM by confocal laser scanning microscopy. In most of the observed cells, ATM partially colocalized with NS3-4A in the perinuclear region and in dispersed points throughout the cytoplasm (Fig. 5A). In particular, we observed prominent colocalization of ATM with NS3-4A in some cells (Fig. 5A). Next, using anti-FLAG and anti-ATM antibodies, we immunoprecipitated lysates from 293FT cells in which FLAG-tagged ATM and either NS3-4A (HCV-O) or NS3 (HCV-O) were overexpressed and then performed immunoblotting analysis using either anti-ATM or anti-NS3 antibody to determine whether ATM binds to NS3-4A or NS3. The results revealed that ATM preferentially bound to NS3-4A over NS3 alone (Fig. 6A). Similarly, we found that ATM bound to NS3-4A using the O cell lysates (Fig. 6B), while HA-tagged Chk2 did not bind to NS3-4A in immunoprecipitation analysis using lysates from 293FT cells in which NS3-4A and HA-tagged Chk2 were overexpressed (Fig. 6C). Although NS3-4A has protease activity, ATM was not cleaved by the NS3-4A protease (Fig. 6D). Taking these results together, we conclude that ATM is able to interact with NS3-4A.

Interaction of HCV NS5B with ATM and Chk2. We next examined the subcellular localization of ATM and/or Chk2 in HCV NS5B-expressing cells by confocal laser scanning microscopy since we previously demonstrated that HCV NS5B-expressing PH5CH8 immortalized human hepatocyte cells were susceptible to DNA damage in the form of dsDNA breaks (23). ATM partially colocalized with NS5B in dispersed points throughout the cytoplasm (Fig. 5B), similar to the subcellular localization of HCV NS3-4A and ATM. Furthermore, Chk2 also partially colocalized with NS5B in the perinuclear region and in dispersed points in the nucleus (Fig. 5C). To determine whether endogenous ATM binds to NS5B, lysates from Oc or

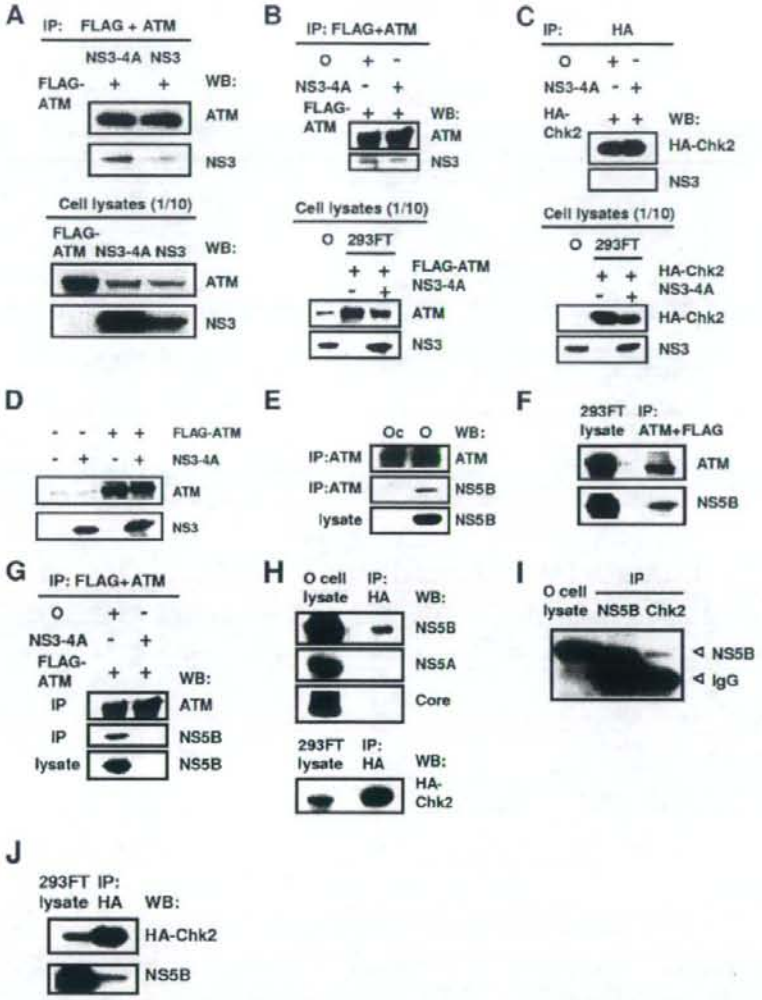

FIG. 6. Interaction of HCV NS3-4A and NS5B with the ATM signaling pathway. (A and B) ATM bound to HCV NS3-4A. (A) 293FT cells were transfected with 4 μg of pCX4bsr/NS3-4A (O), 4 μg of pCX4bsr/NS3 (O), or 4 μg of pcDNA3-FLAG-ATMwt. The cell lysates of expressed FLAG-ATM were mixed with lysates expressing either NS3-4A or NS3. The cell lysates were immunoprecipitated with both anti-FLAG (M2) and anti-ATM (2C1) antibodies, followed by immunoblotting analysis using either anti-ATM (2C1) or anti-HCV NS3 antibody. The results of Western blot analysis of 1/10 of the cellular lysates with anti-ATM or anti-NS3 antibody are also shown. (B) 293FT cells were cotransfected with 4 μg of pcDNA3-FLAG-ATMwt and/or 4 μg of pCX4bsr/NS3-4A (O). The cell lysates of expressed FLAG-ATM alone were mixed with the O cell lysates. Immunoprecipitation and Western blot analysis were performed as described in panel A. (C) Chk2 did not bind to NS3-4A. 293FT cells were cotransfected with 4 μg of pcDNA3-HA-Chk2wt and/or 4 μg of pCX4bsr/NS3-4A (O). The cell lysates of expressed HA-Chk2 alone were mixed with the O cell lysates. The cell lysates were immunoprecipitated with anti-HA antibody (3F10), followed by Western blot analysis using either anti-HA (HA-7) or anti-HCV NS3 antibody. The results of Western blot analysis of 1/10 of the cellular lysates with anti-HA or anti-NS3 antibody are also shown. (D) ATM was not cleaved by HCV NS3-4A protease. 293FT cells were cotransfected with 4 μg of pCX4bsr/NS3-4A (O) and/or 4 μg of pcDNA3-FLAG-ATMwt. The results of Western blot analysis of cellular lysates with anti-ATM or anti-NS3 antibody are shown. (E to G) ATM bound to HCV NS5B. (E) The lysates of O or Oc cells were immunoprecipitated with anti-ATM antibody (2C1), followed by immunoblotting analysis using either anti-ATM or anti-HCV NS5B antibody (no. 14). The results of Western blot analysis of 1/10 of the cellular lysates with anti-NS5B antibody are also shown. (F) 293FT cells were cotransfected with 4 μg of pCX4bsr/NS5B (1B-1) and 4 μg of pcDNA3-FLAG-ATMwt. The cell lysates were immunoprecipitated with both anti-FLAG and anti-ATM antibodies, followed by immunoblotting analysis using either anti-ATM or anti-HCV NS5B antibody. (G) Western Blot analysis was performed with anti-NS5B antibody, reusing the same blotted membrane that was used for panel B. (H to J) Chk2 bound to HCV NS5B. (H) 293FT cells were cotransfected with 4 μg of pcDNA3-HA-Chk2wt. The cell lysates of expressed HA-Chk2 were mixed with the O cell lysates and were immunoprecipitated with anti-HA antibody (3F10), followed by immunoblotting analysis using anti-HCV NS5B, anti-HCV NS5A (no. 8926), anti-HCV core protein (CP-9 and CP-11 mixture), or anti-HA (HA-7) antibody. The results of Western blot analysis of 1/10 of the cellular lysates with the same antibodies are also shown. (I) The lysates of O cells were immunoprecipitated with anti-NS5B or anti-Chk2 antibody (DCS-273), followed by immunoblotting analysis using anti-HCV NS5B antibody. The result of Western blot analysis of 1/10 of the cellular lysates with anti-NS5B antibody is also shown. (J) 293FT cells were cotransfected with 4 μg of pCX4bsr/NS5B (1B-1) and 4 μg of pcDNA3-HA-Chk2wt. The cell lysates were immunoprecipitated with anti-HA antibody (3F10), followed by immunoblotting analysis using either anti-HA (HA-7) or anti-HCV NS5B antibody. IP, immunoprecipitation; WB, Western blotting; IgG, immunoglobulin G.

O cells were immunoprecipitated with anti-ATM antibody, and then immunoblotting analysis using either anti-ATM or anti-NS5B antibody was performed. The results revealed that endogenous ATM bound to endogenous NS5B (Fig. 6E). Furthermore, we confirmed that ATM bound to NS5B in immunoprecipitation analysis using lysates from 293FT cells, in which NS5B (1B-1 strain) and FLAG-tagged ATM were overexpressed (Fig. 6F). Similarly, we confirmed that FLAG-tagged ATM bound to NS5B derived from O cell lysates in immunoprecipitation analysis using lysates from 293FT cells in which FLAG-tagged ATM was overexpressed (Fig. 6G). Finally, to determine which HCV protein binds to Chk2, the 293FT cell lysates of overexpressed HA-Chk2 were mixed with the O cell lysates and were immunoprecipitated with anti-HA antibody, followed by Western blot analysis using anti-HCV NS5B, anti-HCV NS5A, anti-HCV core protein, or anti-HA antibody. Consistent with the immunofluorescence result that Chk2 partially colocalized with NS5B (Fig. 5C), we observed that HA-tagged Chk2 bound to NS5B (Fig. 6H). Importantly, we found that endogenous Chk2 bound to endogenous NS5B derived from O cells (Fig. 6I). In addition, HA-tagged Chk2 bound to NS5B in immunoprecipitation analysis using lysates from 293FT cells in which NS5B (1B-1 strain) and HA-tagged Chk2 were overexpressed (Fig. 6J). Thus, Chk2 also interacted with NS5B as well as ATM. Taking these results together, we conclude that HCV targets ATM and Chk2 DNA damage sensors and that the ATM signaling pathway is required for HCV RNA replication.

DISCUSSION

ATM has been implicated as a target of most DNA viruses, harboring their genomes in the form of dsDNA which can activate or inhibit the ATM signaling pathway (17). In this study, we have demonstrated for the first time that the ATM signaling pathway is required for HCV RNA replication even though HCV does not have a dsDNA genome, unlike DNA viruses. In this regard, Machida et al. previously proposed that HCV infection and the expression of HCV NS3 and core protein induced dsDNA breaks (18, 19). Furthermore, NS3 has DNA helicase activity by which it unwinds dsDNA, suggesting that NS3 affects host dsDNA (22, 25). Thus, HCV infection might trigger the activation of ATM without a dsDNA genome. In fact, we observed weak but significant phosphorylation of Chk2 at threonine 68, the specific marker for ATM activation, in the HCV RNA-replicating cells (O and sO cells) but not in the HCV-negative Oc and sOc cells (Fig. 3A), suggesting that the ATM-dependent DNA damage response is constantly stimulated in persistent HCV RNA-replicating cells. Furthermore, we demonstrated that ATM preferentially bound to NS3-4A over NS3 alone (Fig. 5B) and that ATM partially colocalized with NS3-4A in the perinuclear region, where HCV is known to form a replication complex and replicate itself, and in dispersed points throughout the cytoplasm (Fig. 5A), indicating the interaction of ATM with NS3-4A. Interestingly, Lai et al. very recently reported that NS3-4A impaired DNA repair and enhanced sensitivity to ionizing radiation through interaction with ATM (15). However, we observed an equivalent level of Chk2 phosphorylation at threonine 68, a direct downstream target of ATM (20, 21), in both HCV RNA-replicating cells (O cells) and HCV-negative cells (Oc cells) after treatment with adriamycin (Fig. 3A), suggesting that Chk2 phosphorylation by ATM is not impaired by HCV RNA replication. In this regard, Gaspar and Shenk also showed that human cytomegalovirus could inhibit a DNA damage response by mislocalizing ATM and phosphorylated Chk2 at threonine 68 to a cytoplasmic virus assembly zone, indicating that human cytomegalovirus blocked at the level of Chk2 (9). On the other hand, dsDNA triggers IFN immune defenses through retinoic acid-induced gene I, the mitochondrial antiviral signaling protein, or the DNA-dependent activator of IFN-regulatory factor (7, 26); and NS3-4A protease, which is known to cleave the mitochondrial antiviral signaling protein, can block it (26), suggesting that interaction of NS3-4A with ATM is partially involved in such a common antiviral signaling pathway. On the other hand, we previously demonstrated that HCV NS5B-expressing PH5CH8 immortalized human hepatocyte cells were susceptible to DNA damage in the form of dsDNA breaks (23). In this regard, we have found that HCV NS5B could bind to both ATM and Chk2 (Fig. 5B and C and 6E to J). Together, these results indicate that HCV might hijack ATM and Chk2 and utilize ATM and Chk2 for HCV RNA replication, thereby resulting in impairment of DNA repair, enhancement of mutation frequency, and development of hepatocellular carcinoma.

Finally, consistent with our finding that ATM was required for HCV RNA replication, an ATM kinase inhibitor efficiently suppressed genome-length HCV RNA replication at an EC_{50} of approximately 2 μM at 72 h after the treatment (Fig. 4A). Similarly, Lau et al. reported that the same ATM kinase inhibitor could suppress HIV-1 replication at an EC_{50} of approximately 2.3 μM (16). Importantly, the EC_{50} for HIV-1 replication is similar to that for HCV replication. Thus, this or other ATM kinase inhibitors may represent a novel approach for the clinical treatment of patients with chronic hepatitis C as well as AIDS patients.

ACKNOWLEDGMENTS

We thank D. Trono, R. Agami, R. Iggo, M. Kastan, S. J. Elledge, M. Kohara, A. Takamizawa, and M. Hijikata for the VSV-G-pseudotyped HIV-1-based vector system (pCMVR8.91 and pMDG2) and for pSUPER, pRDI292, pcDNA3-FLAG-ATM, and pcDNA3-HA-Chk2, and for anti-NS3 antibody, anti-NS5B antibody, anti-NS5A antibody, and 293FT cells. We also thank A. Morishita and T. Nakamura for their technical assistance.

This work was supported by a Grant-in-Aid for Young Scientists (B) from the Ministry of Education, Culture, Sports, Science and Technology (MEXT); by a Grant-in-Aid for Research on Hepatitis from the Ministry of Health, Labor, and Welfare of Japan; by the Ichiro Kanehara Foundation; and by a Research Fellowship from the Japan Society for the Promotion of Science.

REFERENCES

1. **Ariumi, Y., P. Turelli, M. Masutani, and D. Trono.** 2005. DNA damage sensors ATM, ATR, DNA-PKcs, and PARP-1 are dispensable for human immunodeficiency virus type 1 integration. J. Virol. **79:**2973–2978.
2. **Ariumi, Y., and D. Trono.** 2006. Ataxia-telangiectasia-mutated (ATM) protein can enhance human immunodeficiency virus type 1 replication by stimulating Rev. function. J. Virol. **80:**2445–2452.
3. **Ariumi, Y., M. Kuroki, K. Abe, H. Dansako, M. Ikeda, T. Wakita, and N. Kato.** 2007. DDX3 DEAD-box RNA helicase is required for hepatitis C virus RNA replication. J. Virol. **81:**13922–13926.
4. **Bridge, A. J., S. Pebernard, A. Ducraux, A.-L. Nicoulaz, and R. Iggo.** 2003. Induction of an interferon response by RNAi vectors in mammalian cells. Nat. Genet. **34:**263–264.

5. **Brummelkamp, T. R., R. Bernard, and R. Agami.** 2002. A system for stable expression of short interfering RNAs in mammalian cells. Science **296:**550–553.
6. **Canman, C. E., D.-S. Lim, K. A. Cimprich, Y. Taya, K. Tamai, K. Sakaguchi, E. Apella, M. B. Kastan, and J. D. Siliciano.** 1998. Activation of the ATM kinase by ionizing radiation and phosphorylation of p53. Science **281:**1677–1679.
7. **Cheng, G., J. Zhong, J. Chung, and F. V. Chisari.** 2007. Double-stranded DNA and double-stranded RNA induces a common antiviral signaling pathway in human cells. Proc. Natl. Acad. Sci. USA **104:**9035–9040.
8. **Dansako, H., M. Ikeda, and N. Kato.** 2007. Limited suppression of the interferon-beta production by hepatitis C virus serine protease in cultured human hepatocytes. FEBS J. **274:**4161–4176.
9. **Gaspar, M., and T. Shenk.** 2006. Human cytomegalovirus inhibits a DNA damage response by mislocalizing checkpoint proteins. Proc. Natl. Acad. Sci. USA **103:**2821–2826.
10. **Harper, J. W., and S. J. Elledge.** 2007. The DNA damage response: ten years after. Mol. Cell **28:**739–745.
11. **Ikeda, M., K. Abe, H. Dansako, T. Nakamura, K. Naka, and N. Kato.** 2005. Efficient replication of a full-length hepatitis C virus genome, strain O, in cell culture, and development of a luciferase reporter system. Biochem. Biophys. Res. Commun. **329:**1350–1359.
12. **Kato, N., M. Hijikata, Y. Ootsuyama, M. Nakagawa, S. Ohkoshi, T. Sugimura, and K. Shimotohno.** 1990. Molecular cloning of the human hepatitis C virus genome from Japanese patients with non-A, non-B hepatitis. Proc. Natl. Acad. Sci. USA **87:**9524–9528.
13. **Kato, N.** 2001. Molecular virology of hepatitis C virus. Acta Med. Okayama **55:**133–159.
14. **Kato, N., K. Sugiyama, K. Namba, H. Dansako, T. Nakamura, M. Takami, K. Naka, A. Nozaki, and K. Shimotohno.** 2003. Establishment of a hepatitis C virus subgenomic replicon derived from human hepatocytes infected in vitro. Biochem. Biophys. Res. Commun. **306:**756–766.
15. **Lai, C. K., K. S. Jeng, K. Machida, Y. S. Cheng, and M. M. Lai.** 2008. Hepatitis C virus NS3/4A protein interacts with ATM, impairs DNA repair and enhances sensitivity to ionizing radiation. Virology **370:**295–309.
16. **Lau, A., K. M. Swinbank, P. S. Ahmed, D. L. Taylor, S. P. Jackson, G. C. Smith, and M. J. O'Connor.** 2005. Suppression of HIV-1 infection by a small molecule inhibitor of the ATM kinase. Nat. Cell Biol. **7:**493–500.
17. **Lilley, C. E., R. A. Schwartz, and M. D. Weitzman.** 2007. Using or abusing: viruses and the cellular DNA damage response. Trends Microbiol. **15:**119–126.
18. **Machida, K., K. T. Cheng, V. M. Sung, S. Shimodaira, K. L. Lindsay, A. M. Levine, M. Y. Lai, and M. M. Lai.** 2004. Hepatitis C virus induces a mutator phenotype: enhanced mutations of immunoglobulin and protooncogenes. Proc. Natl. Acad. Sci. USA **101:**4262–4267.
19. **Machida, K., K. T. Cheng, V. M. Sung, K. J. Lee, A. M. Levine, and M. M. Lai.** 2004. Hepatitis C virus infection activates the immunologic (type II) isoform of nitric oxide synthase and thereby enhances DNA damage and mutations of cellular genes. J. Virol. **78:**8835–8843.
20. **Matsuoka, S., M. Huang, and S. J. Elledge.** 1998. Linkage of ATM to cell cycle regulation by the Chk2 protein kinase. Science **282:**1893–1897.
21. **Matsuoka, S., G. Rotman, A. Ogawa, Y. Shiloh, K. Tamai, and S. J. Elledge.** 2000. Ataxia telangiectasia-mutated phosphorylates Chk2 in vivo and in vitro. Proc. Natl. Acad. Sci. USA **97:**10389–10394.
22. **Myong, S., M. M. Bruno, A. M. Pyle, and T. Ha.** 2007. Spring-loaded mechanism of DNA unwinding by hepatitis C virus NS3 helicase. Science **317:**513–516.
23. **Naka, K., H. Dansako, N. Kobayashi, M. Ikeda, and N. Kato.** 2006. Hepatitis C virus NS5B delays cell cycle progression by inducing interferon-β via Toll-like receptor 3 signaling pathway without replicating viral genomes. Virology **346:**348–362.
24. **Naldini, L., U. Blömer, P. Gallay, D. Ory, R. Mulligan, F. H. Gage, I. M. Verma, and D. Trono.** 1996. In vivo gene delivery and stable transduction of nondividing cells by a lentiviral vector. Science **272:**263–267.
25. **Pang, P. S., E. Jankowsky, P. J. Planet, and A. M. Pyle.** 2002. The hepatitis C viral NS3 protein is a processive DNA helicase with cofactor enhanced RNA unwinding. EMBO J. **21:**1168–1176.
26. **Takaoka, A., Z. Wang, M. K. Choi, H. Yanai, H. Negishi, T. Ban, Y. Lu, M. Miyagishi, T. Kodama, K. Honda, Y. Ohba, and T. Taniguchi.** 2007. DAI (DLM-1/ZBP1) is a cytosolic DNA sensor and an activator of innate immune response. Nature **448:**501–505.
27. **Tanaka, T., N. Kato, M. J. Cho, and K. Shimotohno.** 1995. A novel sequence found at the 3′ terminus of hepatitis C virus genome. Biochem. Biophys. Res. Commun. **215:**744–749.
28. **Thomas, D. L.** 2000. Hepatitis C epidemiology. Curr. Top. Microbiol. Immunol. **242:**25–41.
29. **Wakita, T., T. Pietschmann, T. Kato, T. Date, M. Miyamoto, Z. Zhao, K. Murthy, A. Habermann, H. G. Kräusslich, M. Mizokami, R. Bartenschlager, and T. J. Liang.** 2005. Production of infectious hepatitis C virus in tissue culture from a cloned viral genome. Nat. Med. **11:**791–796.
30. **Zufferey, R., D. Nagy, R. J. Mandel, L. Naldini, and D. Trono.** 1997. Multiply attenuated lentiviral vector achieves efficient gene delivery in vivo. Nat. Biotechnol. **15:**871–875.

Virus Research 137 (2008) 72–79

Contents lists available at ScienceDirect

Virus Research

journal homepage: www.elsevier.com/locate/virusres

A new living cell-based assay system for monitoring genome-length hepatitis C virus RNA replication

Hiromichi Dansako, Masanori Ikeda, Ken-ichi Abe, Kyoko Mori, Kazunori Takemoto, Yasuo Ariumi, Nobuyuki Kato*

Department of Molecular Biology, Okayama University Graduate School of Medicine, Dentistry, and Pharmaceutical Sciences, 2-5-1 Shikata-cho, Okayama 700-8558, Japan

ARTICLE INFO

Article history:
Received 22 February 2008
Received in revised form 6 June 2008
Accepted 6 June 2008
Available online 21 July 2008

Keywords:
Hepatitis C virus
Genome-length HCV RNA
Living cell-based assay
Green fluorescent protein
OGF7 assay system
Anti-HCV reagents

ABSTRACT

We previously developed a cell-based luciferase reporter assay system for monitoring genome-length hepatitis C virus (HCV) RNA replication (OR6 assay system). Here, we aimed to develop a new living cell-based reporter assay system using enhanced green fluorescent protein (EGFP). Genome-length HCV RNAs encoding EGFP were introduced into a subline of HuH-7 cells and G418 selection was performed. One cloned cell line, OGF7, was successfully selected from among the several G418-resistant cell lines obtained, and the robust expression of HCV RNA and proteins in OGF7 cells was confirmed. The fluorescent intensity of OGF7 cells was decreased by interferon- treatment in a dose-dependent manner, and it correlated well with the HCV RNA concentration. We demonstrated that the interferon- sensitivity in the OGF7 assay system measuring the fluorescent intensity was equivalent to that of the OR6 assay system, and that the OGF7 assay system was useful for quantitative evaluation of anti-HCV reagents. The OGF7 assay system is expected to be the most time-saving and inexpensive assay system for high-throughput screening of anti-HCV reagents.

1. Introduction

Persistent hepatitis C virus (HCV) infection frequently causes active liver disease in the form of chronic hepatitis (Choo et al., 1989; Kuo et al., 1989), liver cirrhosis, and hepatocellular carcinoma (Ohkoshi et al., 1990; Saito et al., 1990). HCV infection has now become a serious health problem, with at least 170 million people currently infected worldwide (Thomas, 2000). HCV is an enveloped positive single-stranded RNA (9.6 kb) virus belonging to the *Flaviviridae* (Kato et al., 1990; Tanaka et al., 1995). The HCV genome encodes a large polyprotein precursor of approximately 3000 amino acid (aa) residues, which is cleaved co- and post-translationally into at least 10 proteins in the following order: core, envelope 1 (E1), E2, p7, non-structural protein 2 (NS2), NS3, NS4A, NS4B, NS5A, and NS5B. These cleavages are mediated by the host and virally encoded proteases (Hijikata et al., 1991, 1993; Kato, 2001). NS5B possessing an RNA-dependent RNA polymerase (RdRp) activity is the central enzyme in replication of the HCV genome (Kato, 2001).

In the recent past, interferon (IFN) was used as the main treatment for patients with chronic hepatitis C. Currently, the combination of pegylated-IFN (PEG-IFN) and ribavirin is the standard therapy worldwide, although only 50% of patients show a sustained virological response to this therapy (Hayashi and Takehara, 2006). Several clinical drugs have been proposed as adjuvants to IFN, including cyclosporine A (CsA) (Watashi et al., 2003), mizoribine (Naka et al., 2005), and statins (Ikeda et al., 2006; Ye et al., 2003). Currently, NS3 proteinase/helicase activity and NS5B RdRp activity have been considered as targets for the development of anti-HCV reagents (e.g., the NS3 protease inhibitor BILN 2061 (Lamarre et al., 2003). To date, however, we have not obtained HCV-specific drugs possessing more effective anti-HCV activity than PEG-IFN. Therefore, a more convenient high-throughput screening system is still required to explore more effective anti-HCV reagents.

We previously developed a cell-based genome-length HCV RNA replication system using *Renilla* luciferase as a reporter in order to monitor the HCV RNA replication level (OR6 assay system) (Ikeda et al., 2005; Naka et al., 2005). Other groups have also developed cell-based subgenomic HCV replicon systems using secreted alkaline phosphatase (Yi et al., 2002) or beta-lactamase (Murray et al., 2003) as a reporter. However, these assay systems are still quite time- and cost-intensive methods for measuring enzyme activity.

In the present study, we report a new living cell-based reporter assay system that is able to monitor the level of genome-length HCV RNA replication and to reduce both the time required and the expense.

* Corresponding author. Tel.: +81 86 235 7385; fax: +81 86 235 7392.
E-mail address: nkato@md.okayama-u.ac.jp (N. Kato).

0168-1702/$ – see front matter © 2008 Elsevier B.V. All rights reserved.
doi:10.1016/j.virusres.2008.06.001

2. Materials and methods

2.1. Reagents

IFN- , IFN- , and CsA were purchased from Sigma–Aldrich (St. Louis, MO). IFN- was a gift from Toray Industries (Tokyo, Japan). Fluvastatin (FLV) was purchased from Calbiochem (San Diego, CA).

2.2. Cell culture

Genome-length HCV RNA replicating cells and OR6c cells were maintained as described previously (Ikeda et al., 2005). OR6c cells are cured OR6 cells (Naka et al., 2005) from which genome-length HCV RNA was eliminated by IFN- treatment as described previously (Ikeda et al., 2005).

2.3. Construction of plasmids and RNA synthesis

The plasmids used in this study (Fig. 1A and B) were constructed on the basis of the plasmid pON/C-5B/KE (Ikeda et al., 2005). The plasmid pON/C-5B/KE contains neomycin phosphotransferase (Neo^R) downstream of HCV internal ribosome entry site (IRES) and the full-length HCV-O polyprotein-coding sequence downstream of the encephalomyocarditis virus (EMCV) IRES, and K1609E mutation (Ikeda et al., 2005), was introduced into the NS3 helicase region as the adaptive mutation. The plasmid pOGN/C-5B/KE (Fig. 1A(1)) was constructed from the plasmid pON/C-5B/KE by inserting the PCR product of enhanced green fluorescent protein (EGFP; Clontech Laboratories, Inc., Mountain View, CA) into the AscI recognition site of the 5′-end of the Neo^R gene. The plasmids pON/GC-5B/KE (Fig. 1A(2)) and pON/C-5B G2390/KE (Fig. 1A(3)) were constructed from the plasmid pON/C-5B/KE by inserting the PCR product of EGFP into the XhoI recognition site of the 5′-end of the core-coding sequence and at aa position 2390 (Moradpour et al., 2004) in the NS5A-coding sequence, respectively. Both recognition sites were introduced by PCR mutagenesis with primers containing these recognition sites according to the previously described method (Dansako et al., 2005). To construct the plasmids pOGN/C-5B G2390/KE (Fig. 1B(4)) and pON/GC-5B G2390/KE (Fig. 1B(6)), the EcoRI-SpeI fragments of the plasmids pOGN/C-5B/KE and pON/GC-5B/KE, respectively, were replaced with the EcoRI-SpeI region of the plasmid pON/C-5B G2390/KE. The EcoRI recognition site is located at the 5′-end of HCV IRES, and the SpeI recognition site is located at the 5′-end of the NS3 region within the plasmid pON/C-5B/KE, respectively. To construct the plasmids pOGN/GC-5B/KE (Fig. 1B(5)) and pOGN/GC-5B G2390/KE (Fig. 1B(7)), the EcoRI-RsrII fragment of the plasmid pOGN/C-5B/KE was replaced with the EcoRI-RsrII region of the plasmids pON/GC-5B/KE and pON/GC-5B G2390/KE, respectively. The RsrII recognition site is located in the 3′-end of the Neo^R region within the plasmid pON/C-5B/KE. The obtained plasmids were linearized by XbaI and were used for RNA synthesis with T7 MEGAscript (Ambion, Austin, TX) as previously described (Kato et al., 2003).

2.4. RNA transfection and selection of G418-resistant cells

The transfection of genome-length HCV RNA synthesized in vitro into OR6c cells was performed by electroporation, and the cells were selected in the presence of G418 (0.3 mg/ml; Invitrogen) for 3 weeks as described previously (Kato et al., 2003).

2.5. Visualization of the fluorescence by EGFP

The fluorescence of EGFP was directly visualized by a fluorescence microscope (Axiovert 25CFL; Carl Zeiss) or a confocal laser-scanning microscope (LSM510; Carl Zeiss). The cells were fixed with 4% paraformaldehyde and were photographed under a fluorescence microscope or a confocal laser-scanning microscope as described previously (Dansako et al., 2003).

2.6. Integration analysis

Genomic DNA was extracted from the cultured cells by using a DNeasy Blood & Tissue Kit (QIAGEN, Valencia, CA). The HCV 5′-untranslated region (UTR) and the IFN- gene were detected according to a method described previously (Kato et al., 2003). To test the efficiency of the PCR analysis and the quality of the genomic DNAs, a set of primers was used for the PCR detection of an intronless IFN- gene (1 copy per haploid genome; the expected PCR product is 341 bp).

2.7. Northern blot analysis

Total RNA was extracted from the cultured cells by using an RNeasy Mini Kit (QIAGEN). HCV RNA and -actin were detected according to a method described previously (Ikeda et al., 2005).

2.8. Measurement of the fluorescent intensity in living cells replicating a genome-length HCV RNA with EGFP

The cells replicating a genome-length HCV RNA with EGFP (5×10^4) were plated onto 12-well plates. By using a fluorometer (Fluoroskan Ascent; Thermo Fisher Scientific K.K., Yokohama, Japan), the fluorescent intensity in living cells was measured at 24, 48, and 72 h. In several experiments, the fluorescent intensity in living cells was measured only at 72 h after the treatment with reagents. After the measurements of the fluorescent intensity, the cells were subjected to Western blot analysis for HCV proteins and quantitative RT-PCR analysis for HCV RNA.

2.9. Western blot analysis

The preparation of cell lysates, the sodium dodecyl sulfate-polyacrylamide gel electrophoresis, and the immunoblotting analysis were performed as previously described (Hijikata et al., 1993). Production of core, E1, NS3, NS5A, and NS5B proteins in the O and OGF7 cells was analyzed by immunoblotting using anti-core (CP11; Institute of Immunology, Tokyo, Japan), anti-E1 (a generous gift from Dr. M. Kohara, Tokyo Metropolitan Institute of Medical Science), anti-NS3 (Novocastra Laboratories, Newcastle, UK), anti-NS5A (a generous gift from Dr. A. Takamizawa, Research Foundation for Microbial Diseases, Osaka University), and anti-NS5B (a generous gift from Dr. M. Kohara, Tokyo Metropolitan Institute of Medical Science) antibodies, respectively. Production of EGFP-Neo^R fusion protein was also detected by anti-GFP antibody (JL-8; Clontech). -Actin antibody (AC-15; Sigma) was used as the control for the amount of protein loaded per lane. Immunocomplexes were detected with the Renaissance enhanced chemiluminescence assay (PerkinElmer Life Sciences, Boston, MA).

2.10. Quantitative RT-PCR analysis

The quantitative RT-PCR analysis for HCV RNA was performed by using a real-time LightCycler PCR as described previously (Ikeda et al., 2005).

3. Results

3.1. Establishment of the cloned cell lines replicating a genome-length HCV RNA with EGFP

We previously developed a dicistronic genome-length HCV RNA (O strain of genotype 1b) replication system that stably expresses *Renilla* luciferase as a reporter in order to monitor the level of HCV RNA replication (OR6 assay system) (Ikeda et al., 2005; Naka et al., 2005). To further facilitate mass screening of potential candidates for anti-HCV reagents, we attempted to develop a novel assay system for monitoring the level of HCV RNA replication without lysis of cells. For this purpose, we chose EGFP as a reporter, and we first tried to establish cloned cell lines that efficiently replicate genome-length HCV RNA encoding EGFP. All of the constructed plasmids (Fig. 1) were used as templates for RNA synthesis in vitro, and then the transcribed RNAs were transfected into OR6c cells by the electroporation method, as described in Section 2. After 3 weeks of G418 selection, we obtained several G418-resistant colonies from the OGN/C-5B/KE RNA, ON/GC-5B/KE RNA, ON/C-5B G2390/KE RNA, or OGN/GC-5B/KE RNA-introduced cells, and most of the G418-resistant colonies were successfully established as cell lines (Fig. 1). In contrast, no G418-resistant colonies were obtained from the OGN/C-5B G2390/KE RNA, ON/GC-5B G2390/KE RNA, or OGN/GC-5B G2390/KE RNA-introduced cells (Fig. 1).

To select a cloned cell line showing the highest expression level of EGFP and HCV protein, we first performed Western blot analysis for the detection of EGFP and HCV NS3 protein. The results revealed that OGN/C-5B/KE clone 7, ON/GC-5B/KE clone 3, and OGN/GC-5B/KE clone 3 showed marginally higher expression levels of EGFP and HCV NS3 protein than the other clones (data not shown). Because, in the examination by fluorescence microscopy,

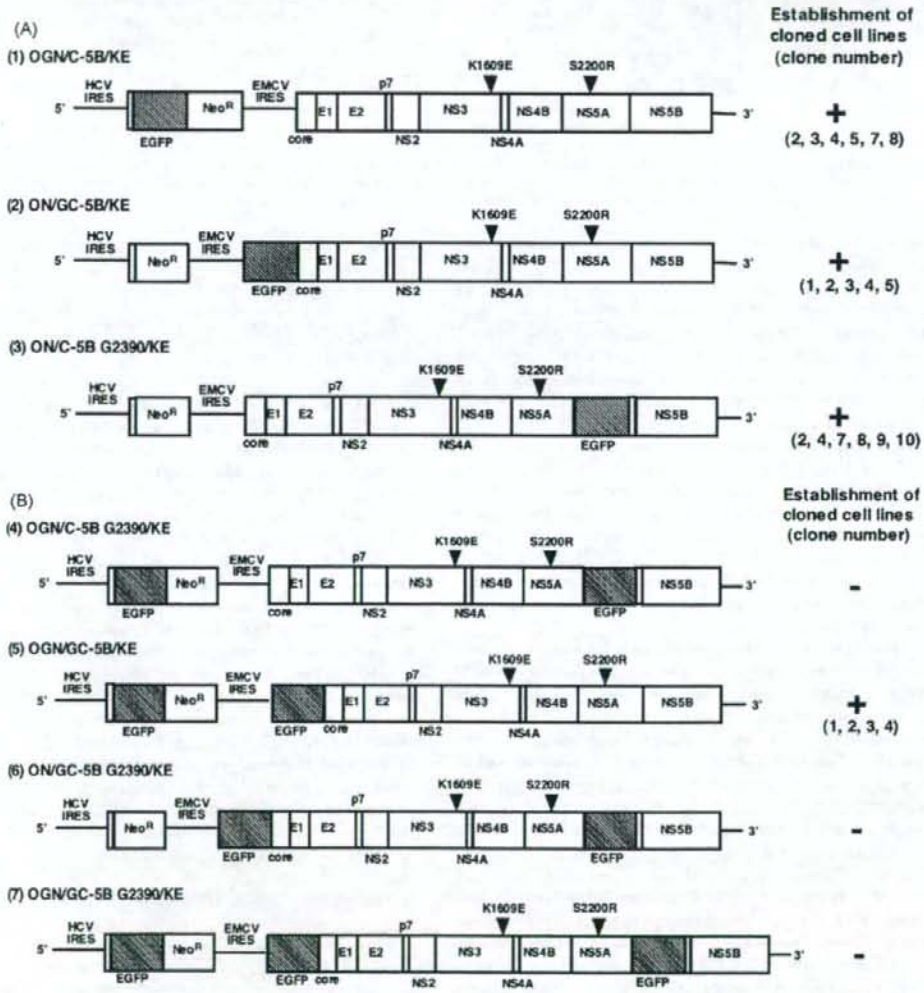

Fig. 1. Schematic presentation of various genome-length HCV RNAs (HCV-O strain) containing an EGFP-encoding sequence. (A) Genome-length HCV RNAs containing one copy of the EGFP-encoding sequence. The basic construct is described in our previous study (Ikeda et al., 2005). The EGFP-encoding region is depicted as a shaded box. Neomycin phosphotransferase is indicated as Neo^R. K1609E and S2200R are adaptive mutations found in previous studies (Ikeda et al., 2005; Kato et al., 2003). (B) Genome-length HCV RNAs containing two or three copies of EGFP-encoding sequence.

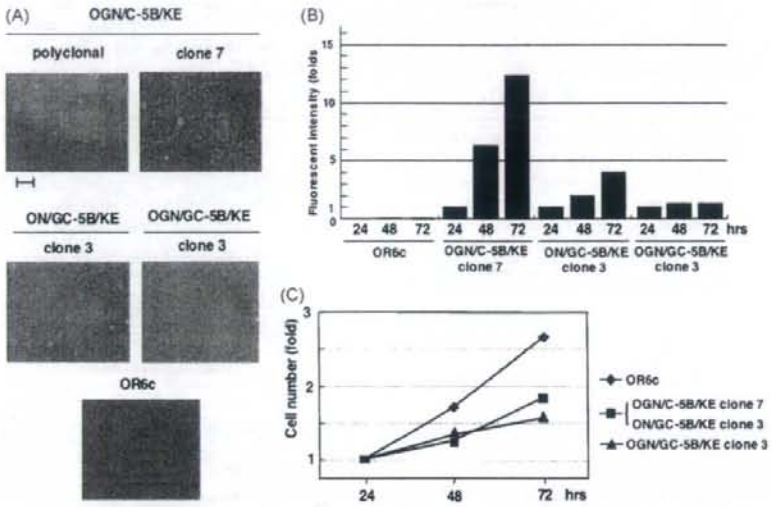

Fig. 2. Fluorescent intensities of G418-resistant cell lines. (A) Visualization of the fluorescence of G418-resistant cell lines under a fluorescence microscope. The panels show the fluorescence of expressed EGFP. Bar, 200 m. (B) Time course of the fluorescent intensity of G418-resistant cell lines. The fluorescent intensity was measured at 24, 48, and 72 h after cell-seeding by a fluorometer as described in Section 2. For calculating the fluorescent intensity in each cell line, the intensity at 24 h after cell seeding was assigned a value of 1. OR6c cells were used as a negative control. (C) Growth curve of G418-resistant cell lines. The cells were plated onto 6-well plate (1×10^5 cells per well), and the kinetics of cell proliferation during 72 h in culture were determined by Trypan blue treatment. OR6c cells were used as a control.

the fluorescence of EGFP in these selected cell lines was roughly equivalent to that in OGN/C-5B/KE polyclonal cells (Fig. 2A), we next examined the time course of the fluorescent intensities of these cells lines by using a fluorometer, and observed a remarkable, twelve-fold increase in the fluorescent intensity of OGN/C-5B/KE clone 7 cells at 72 h after the start of cell culture in comparison with the intensity at 24 h (Fig. 2B). The fluorescent intensity of ON/GC-5B/KE clone 3 cells was slightly increased at 72 h (approximately four-fold). In contrast to these cell lines, the fluorescent intensity of OGN/GC-5B/KE clone 3 cells did not change during the cell culture. Growth curve analysis of these G418-resistant cell lines revealed that these cell clones had a similar kinetics for cell proliferation, although the growth rate of these cell clones was significantly lower than that of OR6c cells (Fig. 2C). These results suggest that the efficiency of genome-length HCV RNA replication in OGN/C-5B/KE clone 7 cells is higher than that in the other clones. Therefore, we finally selected OGN/C-5B/KE clone 7 (herein designated OGF7) for further characterization.

First, to exclude the possibility that the HCV RNA sequence had become integrated into the genomic DNA, we assayed for the HCV 5′-UTR sequence in the genomic DNA isolated from OGF7 cells by PCR. As a positive control, we used a cloned cell line (Mori et al., 2008) in which the HCV 5′-UTR sequence was integrated into the genomic DNA. The HCV 5′-UTR sequence was not detected in the genomic DNA isolated from OGF7 cells, genome-length HCV RNA-replicating O cells (Ikeda et al., 2005), or OR6c cells (Fig. 3A), although an expected product (266 bp or 205 bp) was detected in the positive control (Fig. 3A, lane PC). These results suggest that the HCV RNA sequence (at least HCV 5′-UTR sequence) is not integrated into the genomic DNA in OGF7 cells. Consistent with these results, an approximately 12 kb RNA of the genome-length HCV RNA encoding EGFP in OGF7 cells was also detected by Northern blot analysis, and its accumulation level was almost the same as that in the O cells (Fig. 3B). In addition, we confirmed by Western blot analysis that OGF7 cells efficiently expressed not only HCV proteins but also the EGFP-Neo^R fused protein, and the expression levels of HCV proteins in the OGF7 cells were also equivalent to those in the O cells (Fig. 3C). In summary, these results indicate that the OGF7 cell line harboring replicative genome-length HCV RNA encoding EGFP as a reporter was stably established.

3.2. *OGF7 living cells are useful for direct monitoring of the level of HCV RNA*

First, we examined whether or not the expression level of EGFP in OGF7 cells was sufficient to allow direct visualization by confocal laser-scanning microscopy. As a consequence, we could detect the fluorescence in addition to the core protein expressed in OGF7 cells (Fig. 4). Furthermore, we confirmed that the detected fluorescence was derived from the EGFP expressed in OGF7 cells, because both the fluorescence and the core protein disappeared after IFN- treatment (Fig. 4). These results suggest that the replication of genome-length HCV RNA encoding EGFP-Neo^R fused protein occurs efficiently in OGF7 cells. We next examined whether or not the IFN sensitivity of the EGFP level was associated with that of the HCV RNA level in OGF7 cells. The levels of EGFP and HCV RNA were examined by the fluorometer and real-time LightCycler PCR, respectively. The results revealed that the level of reduction in the fluorescent intensity by IFN- treatment was equivalent to the level of reduction in the HCV RNA level (Fig. 5A and B). In addition, we confirmed by Western blot analysis that the reduction pattern of the EGFP-Neo^R fusion protein by IFN- treatment was also similar to those of the core and NS3 proteins (Fig. 5C). These results indicate that the expression level of EGFP is sufficient for monitoring of the level of HCV RNA, and suggest that the direct measurement of the fluorescent intensity of the living OGF7 cells was an effective means of monitoring the level of HCV RNA replication.

3.3. *The OGF7 system is useful as a quantitative assay system for various anti-HCV reagents*

To clarify whether or not the OGF7 system is useful as a quantitative antiviral assay system, we first compared the IFN- sensitivity of the OGF7 fluorescent reporter system with that

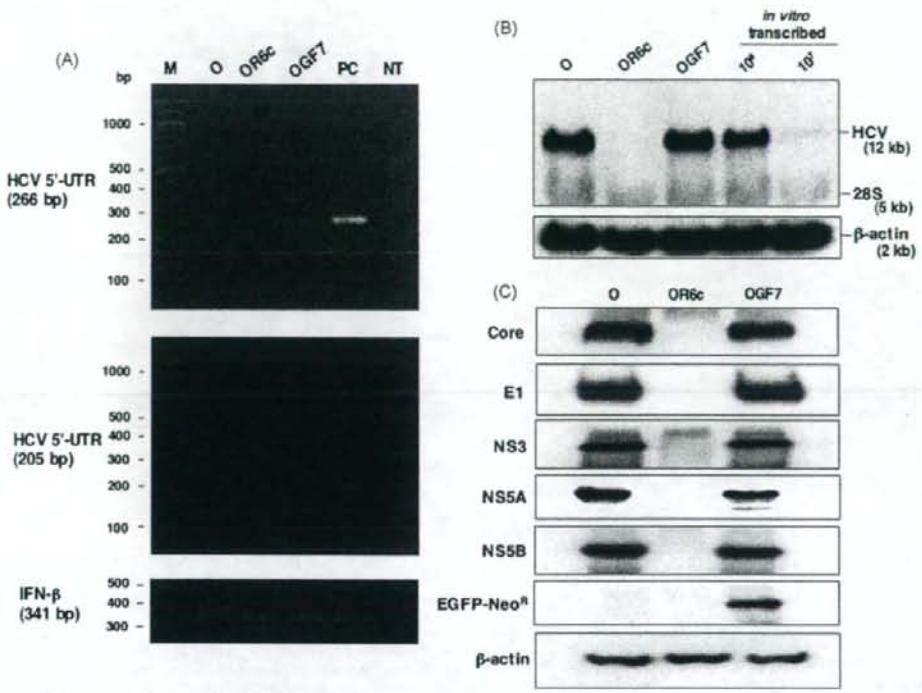

Fig. 3. Characterization of OGF7 cells replicating genome-length HCV RNA encoding EGFP as a reporter. Genome-length HCV RNA-replicating O cells (Ikeda et al., 2005) and OR6c cells (cured OR6 cells) were used for the comparison. (A) HCV genome-derived sequences were not integrated into the genomic DNA from OGF7 cells. Genomic DNA from the OGF7 cells was subjected to PCR for the detection of the HCV 5′-UTR and the IFN- gene. Genomic DNAs from the O and OR6c cells were also used as negative controls. As a positive control, we used genomic DNA from a cell line (Mori et al., 2008) into which the HCV 5′-UTR sequence had been accidentally integrated (lane PC). PCR without genomic DNA was also performed (lane NT). PCR products (266 and 205 bp for HCV 5′-UTR, or 341 bp for the IFN- gene) were detected by staining with ethidium bromide after 3% agarose gel electrophoresis. The 100 bp DNA ladder was used as a size marker (lane M). (B) Northern blot analysis. Total RNAs (3 g each) from the O, OR6c, and OGF7 cells were analyzed by Northern blot analysis using a positive-stranded HCV genome-specific RNA probe (upper panel) and a -actin-specific RNA probe (lower panel), respectively. In vitro-synthesized ORN/C-5B/KE (Ikeda et al., 2005) RNA (10^7 and 10^8 genome equivalents spiked into normal cellular RNA) was used for the comparison of expression levels. (C) Western blot analysis. Production of core, E1, NS3, NS5A, and NS5B proteins in the O and OGF7 cells was analyzed by immunoblotting using anti-core, anti-E1, anti-NS3, anti-NS5A, and anti-NS5B antibodies, respectively. Production of EGFP-Neo^R fusion protein and -actin was also detected by anti-GFP and anti- -actin antibodies, respectively.

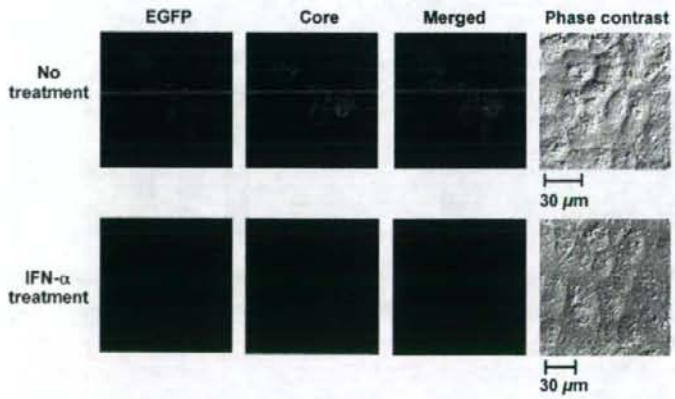

Fig. 4. The EGFP and core protein expressed in OGF7 cells disappeared following IFN- treatment. OGF7 cells were examined by confocal laser-scanning microscopy. Cells were treated with IFN- (500 IU/ml for 6 h). The cells were visualized with a fluorescence microscope, and then the cells were stained with anti-core antibody (CP11; Institute of Immunology, Tokyo, Japan) and Cy3-conjugated anti-mouse secondary antibody (Jackson Immuno Research, West Grove, PA) according to a method described previously (Naka et al., 2006). The merged panels show the two-color overlay images. Bar, 30 m.